Marine and Petroleum Geology 168 (2024) 107042

Contents lists available at ScienceDirect

Marine and Petroleum Geology

journal homepage: www.elsevier.com/locate/marpetgeo

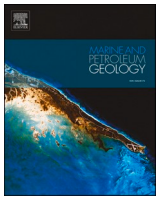

# Interaction between basement detachment fault, rift onset unconformity, and overlying basin fills: An example from the Songliao basin of a Cretaceous active continental margin volcanic rift in northeast Asia

Pujun Wang [a,*], Zhuolong Yang [a], Youfeng Gao [b], Xuejiao Qu [c], Haibo Liu [a], Yongkang Yin [a], Chengshan Wang [d], Xiaoqiao Wan [d], Shumin Chen [e]

[a] College of Earth Sciences, Jilin University, Changchun 130061, China
[b] Research Center of Palaeontology and Stratigraphy, Jilin University, Changchun 130026, China
[c] School of Petroleum and Gas Engineering, Chongqing University of Science and Technology, Chongqing 401331, China
[d] State Key Laboratory of Biogeology and Environmental Geology, School of Earth Sciences and Resources, China University of Geosciences Beijing, Beijing 100083, China
[e] Institute of Exploration and Development of Daqing Oilfield Company Ltd., Daqing 163712, China

ARTICLE INFO

*Keywords:*
Songliao basin
Tectonics
Rift onset unconformity
Detachment fault
Basement sequence
Triassic
Sedimentation rate
Cretaceous

ABSTRACT

How does a giant rift basin begin? No precise examples describe this issue. Based on 7108 m of continuous coring data recovered from the whole stratigraphy of the Songliao Basin (SLB), an attempt has been made to answer this question. Through comprehensive geological, geochemical and seismic research it has been found that there is a triangular extensional domain (TED) beneath the sedimentary cover in the basement at the rift center, from where the initial rupture of the giant rift was created. The basement detachment fault (DF), rift onset unconformity (ROU), and overlying basin fills are interrelated elements of a sedimentary basin and are the key to interpreting the geological archives recorded in the basin. The interaction processes between them determine the location of the basin center and the style of basement subsidence, which reflect the tectonic properties of the basin. This interaction may have a coevolutionary relationship with the deep magmatic activities beneath the basin. The basement of a basin typically consists of a series of strata that the lower strata age older. The uppermost basement sequence of the Triassic in the SLB is particularly important for the overlying basin formation and evolution. The surface topography controlled the thickness of the overlying Cretaceous cover. An ROU and DF developed at the top and bottom of the Triassic, respectively.

The long-term uplift, denudation, and subsequent volcanic deposition may be common features of an ROU in a volcanic rift basin. More so, DF is the controlling factor for basin subsidence in the syn-rift stage of basin evolution. The frequent intrusive association with graben faults suggests that sublithospheric mantle flow may affect the accommodation space of the overlying basin by cutting the basement blocks via feeder dykes and shaping the graben pattern on top of the basement.

## 1. Introduction

In order to investigate geological properties of the early rifting process in an active continental margin volcanic rift basin, an international continental scientific drilling project (ICDP), a deep borehole, known as well SK2, was drilled at the center of the Songliao Basin (SLB) in northeast China (Figs. 1 and 2), which provides A series of high-resolution continuous geological data recording the basin-filling history in the SLB. This borehole represents the deepest continuously cored ICDP borehole to date, with a bottom depth of 7108 m below the surface and a high core yield of 96.61% (Wang et al., 2024). The basement of a basin is defined as the rock assemblage beneath the sedimentary cover of interest. These blocks existed before the overlying basins were formed and filled. The SLB is the first sedimentary basin in the world in which an entire basin sequence from the surface to the metamorphic basement has been drilled, and a continuous complete core section has been obtained (Wang et al., 2021). The SLB was previously thought to have developed on the Hercynian basement and accumulated continuous sedimentary

* Corresponding author.
*E-mail address:* wangpj@jlu.edu.cn (P. Wang).

https://doi.org/10.1016/j.marpetgeo.2024.107042
Received 10 December 2023; Received in revised form 31 July 2024; Accepted 31 July 2024
Available online 2 August 2024

deposits during the Jurassic and Cretaceous (Wan et al., 2013; Wang et al., 2016; Feng and Graham, 2023). However, new data indicate that the SLB basement is a multi-layered succession composed of Triassic and Late Paleozoic sequences. Thick Cretaceous petroliferous sequences were deposited directly on the volcanic-sedimentary strata of the Triassic basement (Yin et al., 2019) after a hiatus spanning the Jurassic (Liu et al., 2021). These propel the need for reconsideration of the Mesozoic tectonic evolutionary history of the SLB and even Northeast Asia. In other words, when did such a giant rift basin open? How did it start? What are the key geological processes that occurred during the initial rifting process? The answer to the scientific question behind the events and phenomenon lies in the process by which a volcanic rift basin is initially ruptured. In this study, the geological properties of the early rifting process in the SLB based on the latest research results of Well SK2 continuous core sections coupled with cross-well 3D seismic data have been revealed. The timing of the rift onset is generally evidenced by a major uplift and erosional event that preceded the rift phase and resulted in a widespread hiatus caused by erosion and peneplanation (Franke, 2013). Because most ROUs have sunk to the seafloor, there is hardly a detailed example of how an ROU is formed. How does a basement weakness become a rifting center in the first step? Rift location is a key feature of continental rift evolution from the initiation to incipient breakup. This is most likely controlled by the reactivation of a lithospheric-scale basement weakness, as described by Corti (2009). However, only a detailed characterization of the process of rift center formation will help in understand the initial evolution of continental rifts. Indications from Davis and Lister (1988) show that DFs juxtapose younger over older, or structurally higher over structurally lower rocks and that they commonly separate upper-plate unmetamorphosed or low-grade metamorphic rocks from lower-plate crystalline rocks of a higher metamorphic grade; the latter commonly have mylonitic fabrics. In structural geometry, DFs are complex 3D systems that change configuration during their evolution, perpetually controlling the associated basin formation, footwall configuration, subsidence, and uplift patterns (Gresseth et al., 2023). Therefore, it is important to know the relationship between basement DFs and the formation and evolution of the overlying basins. It is necessary to understand the response relationship between the deep basement fault system and overlying basin filling. It is found that the initial rupture center of the SLB is composed of a triangular extentional domain (TED) which was created by the interaction between the basement DFs and the ROUs associated with mantle-derived deep intrusions. The filling pattern and subsidence rate of the overlying basin were controlled predominantly by the three interrelated factors of the DF, ROU and volcanism in the deep basin. Cretaceous DFs and graben basins are widely distributed throughout Northeast Asia (Fig. 1a and Ma et al., 2024), which is an ideal natural laboratory for testing different models of basin dynamics concerning the interaction between basin-forming elements. After studying the Early Cretaceous Hohhot metamorphic core complex (HMCC) and its master Hohhot detachment fault (HDF), Davis et al. (2002) concluded that the

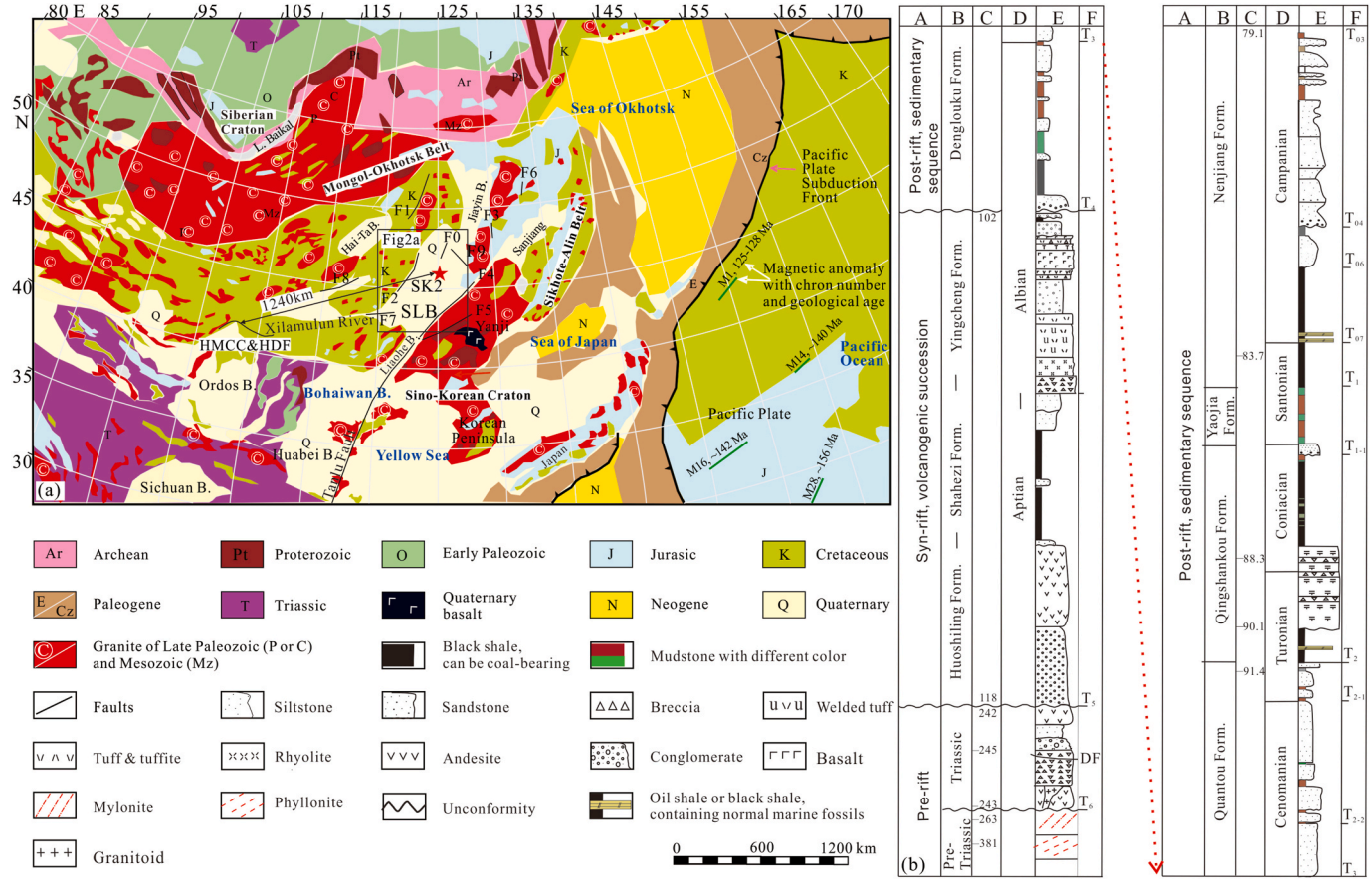


**Fig. 1.** Tectonics and stratigraphy of the Songliao Basin (SLB); modified after Ren et al. (2013); Wang et al. (2016). Ages in (b) compiled from this study and Wan et al. (2013). (a) Regional geological map of Northeast Asia with the SLB located in the center. (b) Syn-rift and post-rift tectono-stratigraphic successions of vertical basin fill sequence of the SLB, A-Tectonic basin filling stage; B-Formation; C-Ages; D-Epoch; E-Stratigraphic column; F-Seismic reflector.The red star shows the location of the international continental scientific drilling project (ICDP) deep borehole named SK2 which is 1240 km northeast (57.62° east by North) of the Hohhot metamorphic core complex (HMCC) and the master Hohhot detachment faults (HDF) (Davis et al., 2002). Other faults are: the Tayuan-Xijiatu Suture Zone (F1); Nenjiang-Balihan Fault (western boundary fault of the SLB) (F2); Mudanjiang Suture Zone (F3); Jiamusi-Yitong Fault (eastern boundary fault of the SLB) (F4); Dunhua-Mishan Fault (F5); Lower Heilongjiang or Dahezhen Fault (F6); Xilamulun River - Changchun-Yanji Suture Zone (F7); and Heihe-Hegenshan Suture Zone (F8). The central fault systems of the SLB are composed of NW-SE toN-S (F9) and SW-NE (F0) faults.

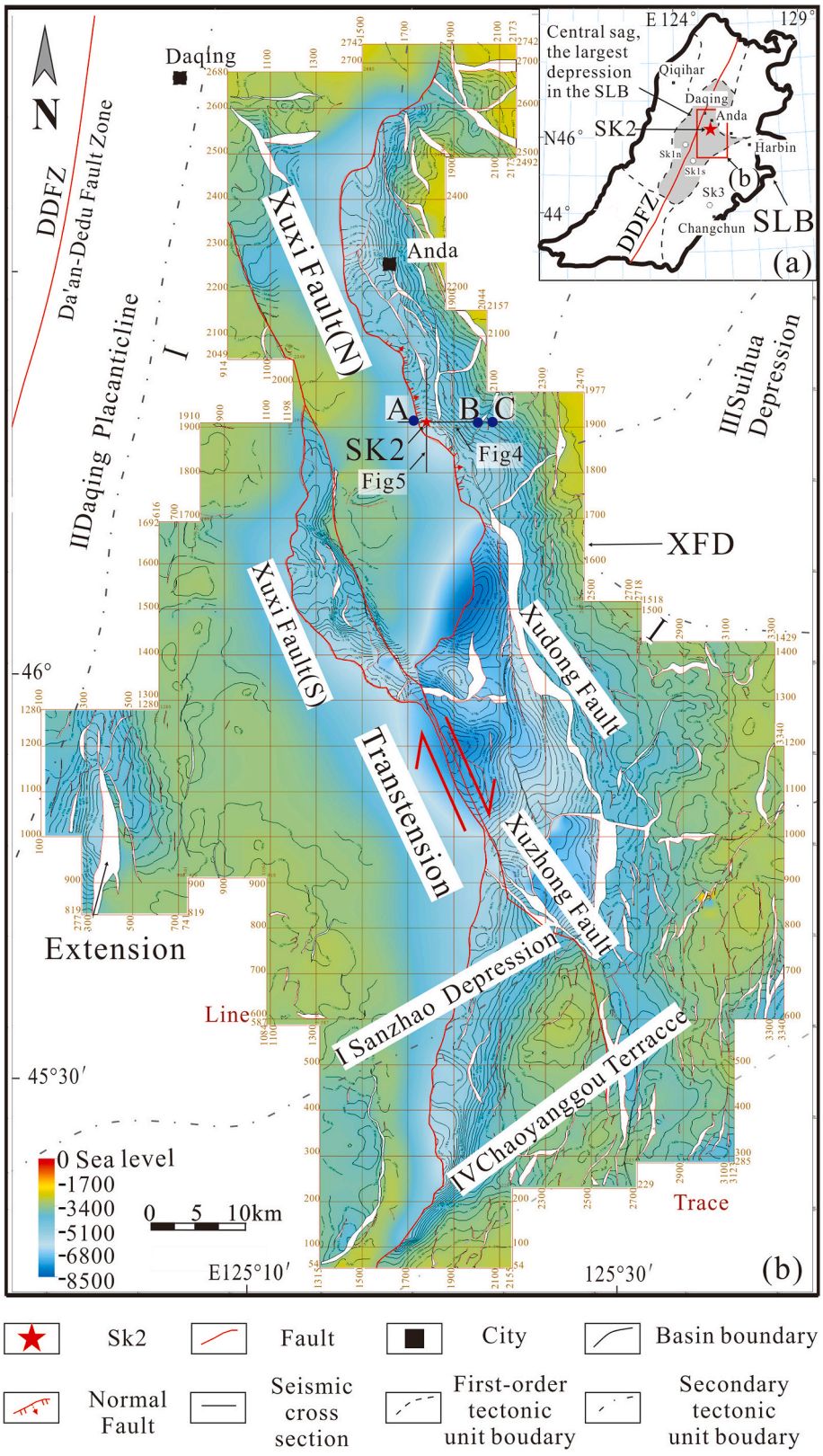


**Fig. 2.** Location map of the Songliao Basin (SLB) and the ICDP borehole SK2 (coordinates E 125°21′47.03″; N 46°14′26.89″, ground altitude 164 m above mean sea level). (a) The SLB showing the largest Upper Cretaceous depression of the central sag was developed in the middle of the basin. (b) Buried depth contour map of the rift onset unconformity (ROU-T5) in the central SLB based on borehole-constrained 3-D seismic data (The seismic line spacing is 50m, and the trace spacing is 25m). The Xujiaweizi fault depression (XFD) is the largest rift structure of the Lower Cretaceous in the SLB. The depression was developed on the deepest area of the underlying Triassic basement blocks and controlled by the basement central fault systems of the Xuxi (west), Xuzhong (middle) and Xudong (east) faults. The Roman numerals I-IV indicate the distribution of the Upper Cretaceous depressions which are not bounded by the basement faults. The three points of A, B and C on the profile line cross well SK2 correspond to the extensional fault points of A, B and C in the seismic profile of Fig. 4b.

intraplate extension began between 125 and 121 Ma after the end of the major Early Cretaceous contraction in Northeast Asia. This event can be reasonably attributed to the gravitational collapse of the orogenically thickened crust. Gravitational collapse may also have been facilitated by the Early Cretaceous intrusion of granitic plutons (ca. 137–119 Ma). It would be interesting to determine whether there is any relationship between the initial rifting of the SLB and the extension of the HDF regional fault. This is of great significance for studying the Cretaceous regional extension and basin formation mechanisms in Northeast Asia (Fig. 1a; Ma et al., 2024). It is generally believed that the control of a DF over a basin is mainly manifested as migration of depocenter in the basin. With the extension of the DF, the depositional center of the overlying basin has been predicted to migrate upward along the sliding surface of the DF. It is the case in the evolution model of the Hohhot supradetachment basins (HSDB) in Inner Mongolia of northeast China which is in the same tectonic setting of the SLB during the Late Mesozoic (Fig. 1a; Ritts et al., 2010). However, our study indicates that the investigation of the interrelated elements between DF, ROU and subsiding center is necessary to unravel the mechanism of Cretaceous rift basin formation. In contrast to the HSDB, migration of the SLB subsiding center along the basement DF occurred only in the beginning stage of the initial rifting before the formation of a ROU and lasted only a couple of million years. After that, the center of the basin remained fairly stable near this initial center of subsidence for a long period of time, lasting for more than ten to thirty million years.

## 2. Geologic setting

The SLB covers an area of approximately 260,000 km$^2$ in Northeastern Asia and preserves a continuous and complete Cretaceous terrestrial record (Wang et al., 2021). This is the most important petroliferous sedimentary basin in China with the continuous annual equivalent oil and gas production of tens of millions of tons (ca. 220–440 million barrels per year) since the 1960s (Wang and Chen, 2015; Daqing oil and gas region compilation committee, 2023). In the Late Mesozoic, the SLB was located in a two-sided, active continental margin tectonic setting. (Fig. 1a). That was characterized by the active orogenic belts of the northern/northwestern Mongol–Okhotsk and the eastern Sikhote-Alin belts during the Late Mesozoic. The Pacific Ocean displays an aging seafloor, becoming older from the Cenozoic to the Jurassic with increasing distance from the continental margin, showing a "non--Andean" type of continental margin (Wang et al., 2016, Fig. 1a). The Cretaceous basin-fills include three tectono-stratigraphic sequences composed of the syn-rift, post-rift, and structural inversion sequences (Fig. 1b). The syn-rift stage is characterized by widespread fault-bounded grabens and volcanogenic successions, which correspond to the upward Lower Cretaceous Huoshiling, Shahezi, and Yingcheng Formations. A giant united sedimentary sag basin characterized the post-rift stage. The sequence **i**ncludes the Lower to Upper Cretaceous Denglouku, Quantou, Qignshankou, Yaojia, and Nenjiang Formations. In the structural inversion stage, the basement stretching stopped abruptly at approximately 79.1 Ma, which was recognized by the regional seismic reflection truncation interface of T03 (Fig. 1b)**.** This sequence includes the Upper Cretaceous Sifangtai and Mingshui Formations. During this stage, there was a continuous depocenter migration from southeast to northwest. The basin shrank to demise due to the changes in the subduction parameters of the Pacific subduction zone (Wang et al., 2016).

## 3. Materials and methods

All the continuously cored geological records from the surface to 7108 m depth in Well SK2 were used in this work. On-site core processing included surface scanning, routine observation, and description in centimeter scale for all the collected cores, which were cut down in the middle, half for permanent storage and observation and the other half for sampling. Laboratory work included microscopy analysis and elemental and isotope analyses of the selected samples. Borehole-constrained 3D seismic, well-logging, and logging datasets are used. High-precision core image scanning was completed within 48 h after the cores were released from the wellbore by the logging team of the Daqing Oilfield Geological Logging Company using a CORESCAN digital core scanner (DMT GmbH & Co. KG in Germany). Synthetic seismogram is used to tie the SK2 well data (depth domain) with the seismic data (time domain). The logging curve data used in this study are obtained from the international continental scientific drilling project (ICDP) well of SK2 in the Songliao Basin (SLB). The 3D seismic data are obtained from the latest interpretation results of the Daqing Oilfield Exploration and Development Research Institute. A PetrelTM 2018 (Schlumberger, 2018) software developed by the Schlumberger group is used to load the AC (acoustic impedance) and DEN (density) curves to extract the wavelets. Those wavelets are correlated with the wavelets from the SK2 well-side channel in the 3D seismic data to establish a time-depth correspondence. Then the linear function tool in the PetrelTM software is used to generate a time (x)–depth (y) conversion equation. The relationship is expressed as $y = 0.5203x + 215.78$, and the corresponding correlation coefficientt ($R^2 = 0.9896$) was obtained. This indicates a good fit and high reliability. Thus, the depth domain in Figs. 4 and 5 is calibrated by using both the SK2 well depth measurements and the further refined independent result through calculations referencing various data sources of drilling footage and synthetic seismogram. It is a precise and reliable time domain and depth domain relationship. The U-Pb zircon dating was carried out at the Key Laboratory of Mineral Resources, Jilin University, Changchun, China. the working conditions are the GeoLasPro 193 nm ArF excimer laser (Compex Systems Pte. Ltd, Germany) and the Agilent 7900 plasma mass spectrometer (Agilent Technologies Co. Ltd., United States), with a beam spot diameter of 32 μm. For every five sample points, one zircon 91500 and one NIST 610 were measured. Age was calculated using standard zircon 91500 as the external standard for the isotope ratio fractionation correction. The buried depth contour of the ROU in the central SLB is mapped based on borehole-constrained 3-D seismic data (Fig. 3b) by tracing the seismic reflection interface of T5 developed in the region, as defined in column F in Fig. 1b.

## 4. Results

### 4.1. Multi-layered basement system and brittle-ductile transition zone

The SK2 borehole encountered and obtained a total of 1148 m of continuous intact basement cores from a buried depth of 5960–7108 m (Figs. 3 and 4). The basement assemblage is composed of multi-layered successions of Triassic and Late Paleozoic sedimentary, volcanic, and metamorphic rocks (Fig. 3). During the coring operations, we found several other basement layers composed of Paleozoic mylonite and phyllonite beneath the Triassic basement (5960–6960 m below the surface). These Triassic and Paleozoic successions form a multi-stratum basement in the Songliao Basin (SLB). Unconformities are frequently observed between the stratigraphic units. At the bottom of the Triassic sequence (well depth 6960 m), a major regional unconformity was developed between the Triassic and Paleozoic successions, which was identified as the Paleozoic basement–Triassic boundary (BP\T, Fig. 3), which represents the brittle–ductile transition. Above the BP\T, the rocks exhibit brittle fabrics. These rocks are the Middle Triassic brecciated andesite (dated to 245.0 ± 1.7 Ma, well depth 6453.17 m, core sample 1) and the granite porphyry (243.8 ± 2.5 Ma, well depth 6958.38 m, core sample 2). Below the BP\T interface is a metamorphic complex composed of mylonite and phyllonite with ductile fabric (Fig. 3). The mylonite (core sample 3) was derived from metamorphosed Guadalupian pyroclastic rocks (crystal-rich, dated to 263.2 ± 8.8 Ma, well depth 6973.1 m). The phyllonite (core sample 4) was derived from metamorphosed Upper Devonian siliceous clastic rocks (dated to 381.1

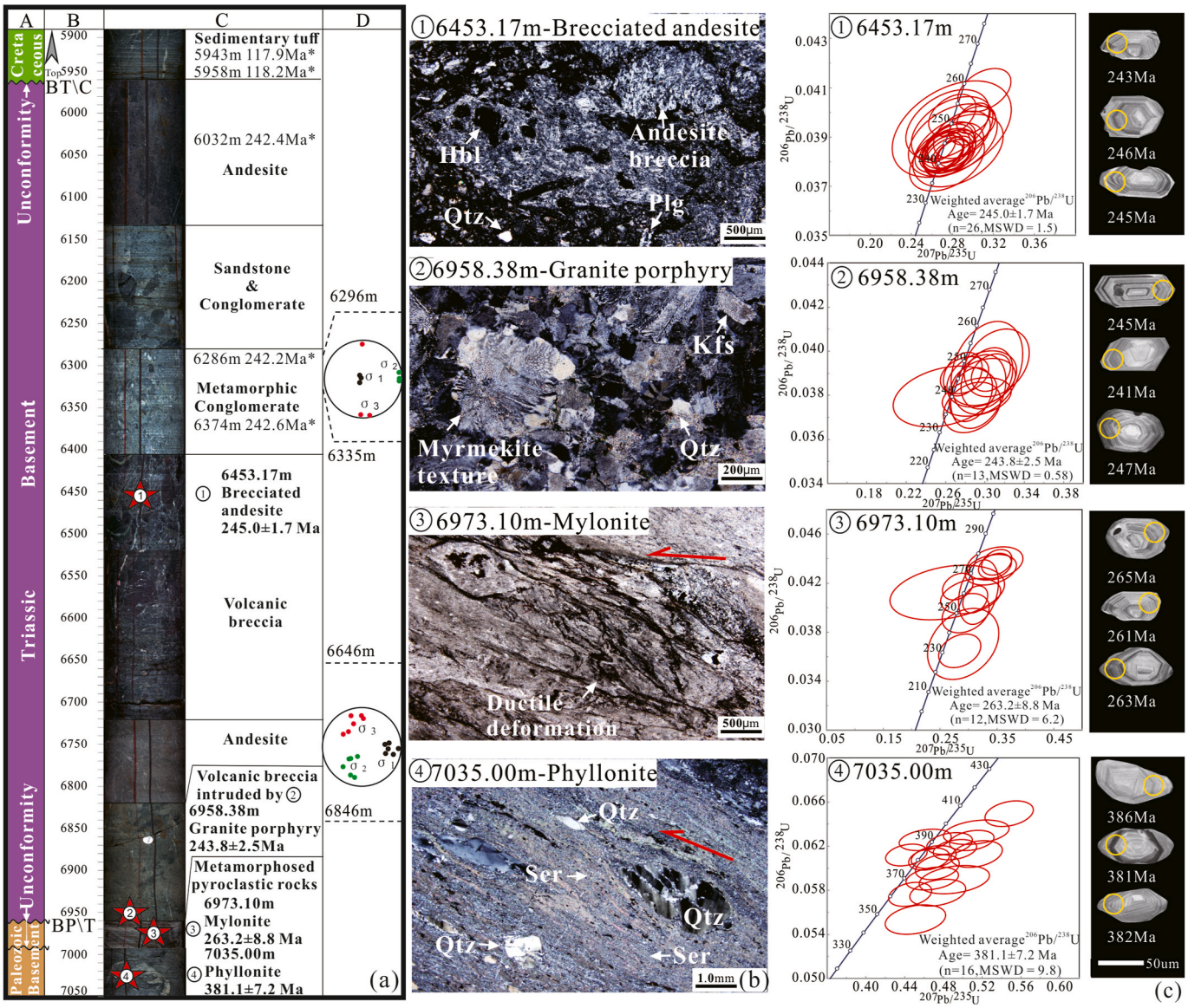


**Fig. 3.** Multi-layered basement of the Triassic and Paleozoic strata and age data of the Songliao Basin (SLB) revealed by the ICDP borehole SK2. (a) Stratigraphic framework of the basement sequence. A-Period; B-Depth in meters below the surface; C-Stratigraphic column shown by surface scanning image of the SK2 core sections, D- In-situ stress measurements in the SK2 borehole from literature (Wang et al., 2020). The five asterisked ages above 6400 m are from our previous studies (Yin et al., 2019; Liu et al., 2021). (b) Photomicrographs (cross-polarized light) of zircon U–Pb dated core samples corresponding in depth to those in the right diagram (c). Mineral abbreviations: Hbl-Hornblende, Plg-Plagioclase, Kfs-K-feldspar, Qtz-Quartz, Ser-Sericite. The red arrows in (b) indichate top-left or sinistral (counterclockwise) rotation deformation of ductile shear scence.(c) Zircon U–Pb dating Concordia diagrams (data corresponding to Table 1).

± 7.2 Ma, well depth 7035 m). The time gap between samples 3 and 4 is approximately 117.9 Myr (263.2–381.1 Ma). The basement section generally exhibits a normal downward aging sequence (Fig. 3). The fact that the granite porphyry (243.8 ± 2.5 Ma) is younger than its overlying andesite (245.0 ± 1.7 Ma) suggests that the basement successions must have been intruded and modified frequently by Subsequent magmatic activities. It is believed that if a hole is drilled sufficiently deep, a similar multi-layered downward aging sequence of the basement strata may be revealed in any basin.

### 4.2. Detachment fault (DF)

The SK2 borehole is located in the center of the SLB, 1240 km northeast (57.62° east by north) of the HMCC and HDF (Fig. 1). This revealed a DF system in the SLB at well depths of 6490–7108 m. At the same location, both the ROU at 5960 m and the corresponding overlying basin fills of 2988 m thickness at a buried depth of 5960–2972 m were continuously cored (Figs. 2–4). The influence of the underlying basement on the filling of the overlying basin is usually realized through basement relief, as shown in Fig. 2b. The basement DF in the shear zone, approximately 618 m thick, was drilled through a depth of 6490–7108 m in the SK2 borehole (Figs. 3 and 4). The top of the DF is at a buried depth of 6490 m, corresponding to a layer of Middle Triassic brecciated andesite (core sample 1, Fig. 3) Feng and Graham, 2023; Yu et al., 2020, which is underlain by interbedded formations of Late Paleozoic mylonite and phyllonite (core samples 3 and 4, Fig. 3). The Paleozoic metamorphic core complexes show distinct ductile deformation fabrics, and they must have been intruded/modified by the granite porphyry (core sample 2, Fig. 3). The strongest seismic reflector in the shear zone of the DF system corresponds to the unconformity boundary between the Triassic and Paleozoic strata, which is the brittle–ductile transition zone (BP\T) at 6960 m below the surface (compare Figs. 3 and 4).

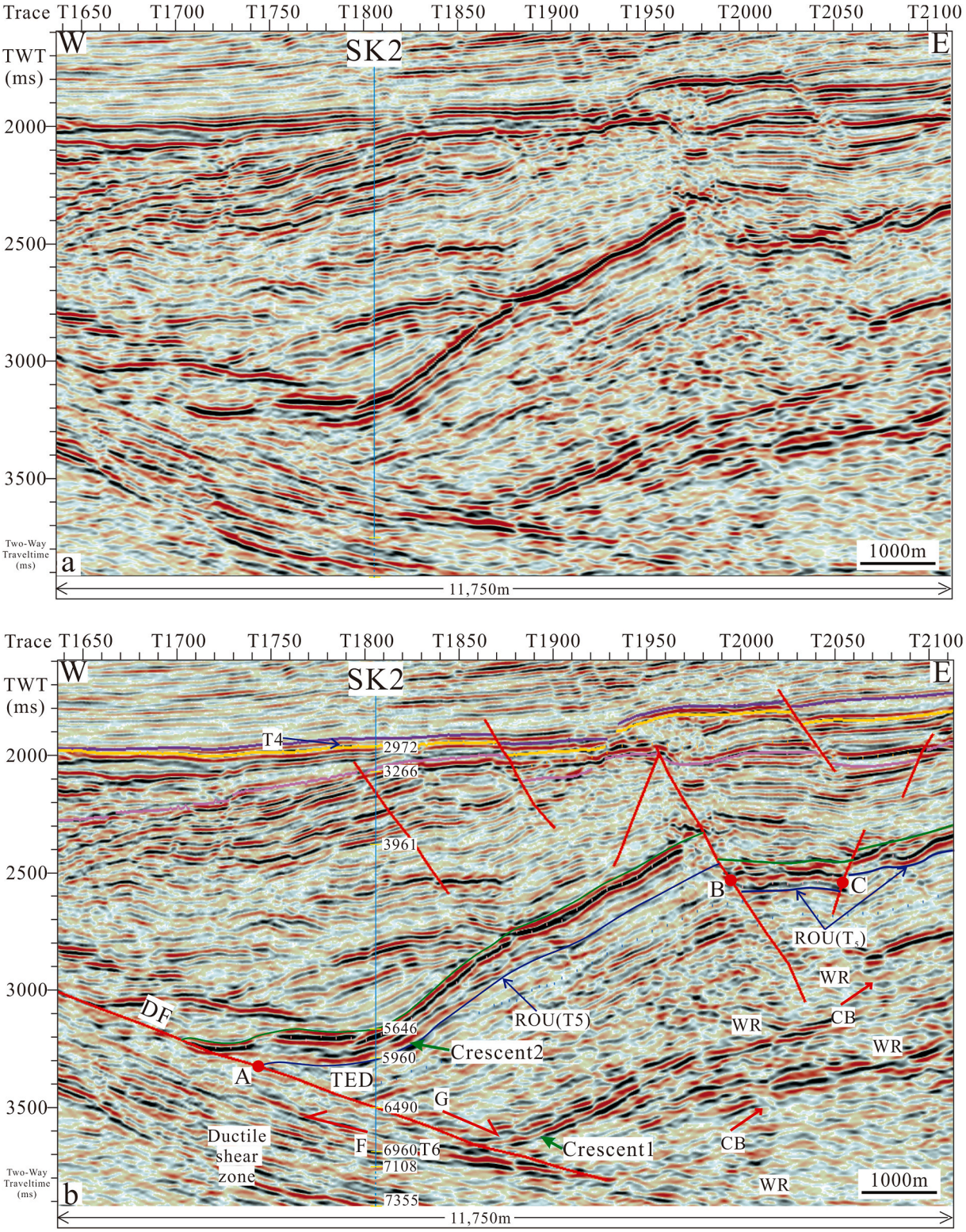


*(caption on next page)*

**Fig. 4.** Seismic profiles through the well SK2 from west to east. (a)- non-interpreted seismic profile and (b)- interpreted seismic section corresponding to a. The profile lines on plan view are shown in Fig. 2b. The profiles show the relationship between the basement detachment fault (DF), rift onset unconformity (ROU), triangular extentional domain (TED) of the initial rifting center and overlying basin fills of the SLB. The vertical line and numbers represent the location and depth meter of the borehole underground. The lithology of the well SK2 at each depth section is shown in Fig. 3a. The seismic reflectors of T4, T5 and T6 correspond to those of Fig. 1b. The high-angle thick red lines represent graben faults. The graben fault points A, B and C in the profile (b) correspond to the extensional fault points A, B and C on the contour plan of Fig. 2b. The ROU is at a depth of 5960 m corresponding to the unconformity interface between the Cretaceous cover and Triassic basement identified as BT\C in Fig. 3a. The bottom of the Triassic sequence is at the depth of 6960 m corresponding to the unconformity boundary between the Triassic and Paleozoic successions identified as BP\T in Fig. 3a. The intersection depth of the DF and Well SK2 is at 6490 m being in the middle lower part of the kilometer-thick Triassic basement strata (530 m above, 470 m below). Note that (1) the bold arrow-G indicates the top-right dextral (clockwise rotation) mass movements of the hanging wall rocks. (2) Arrow-F indicates the top-left sinistral (counterclockwise rotation) deformations of the strata under the DF. (3) WR indicates the worm-like or snake-like shaped reflections moving upward, cutting through wall rocks in the way. They are most likely the remnants of the upward-going magma, known as feeder dykes. (4) Arrow-CB indicates the captured wall rock blocks enclosed in the feeder dykes. (5) The crescents 1 and 2 indicate a series of down-warping sags climbing upwards along the gliding surface of the DF. The crescent-shaped deposit with the greatest curvature is located right in the center of the basin where we drilled the borehole SK2.There is a triangular extensional domain (called TED) recognized by the three points of A on the DF, 5960 m on the ROU and 6490 m on the DF in Fig. 4b. Note that the TED is beneath the ROU, in the basement strata, at the basin center. It is suggested that the TED is probably the cradle of this giant rift structure, the starting point of the initial rift in the SLB. There is a counterpart of the TED which is recognized by the three points of DF, borehole depth of 5960 m and 6490 m in Fig. 5b. Because the stretching direction of the TED shown in Fig. 4b is from west to east, while that shown in Fig. 5b is from south to north, the extensional direction of the regional stress field is from southwest to northeast during the initial rifting of the SLB. That is consistent with the direction from the Hohhot detachment faults (HDF) to the well SK2 (see the position relationship in Fig. 1a). Thus it is suggested that the basement extensional fault (DF) that led to the formation of SLB initial rifting may have a coevolutionary relationship with the HDF in the Early Cretaceous.

#### 4.2.1. Deformation of the hanging wall

As shown in Figs. 3 and 4, the top of the multi-layered basement sequence is composed of kilometer-thick Triassic strata at a buried depth of 5960–6960 m, which were cut by the DF of the basin through its middle lower part (530 m above and 470 m below). The strata of more than 100 m thickness above the fault plane at a burial depth of 6490–6385 m show a top-right shear sense (see bold arrow G in Fig. 4b). This shows that the strata overlying the fault plane have the characteristics of gravitational collapse along the gliding surface of the fault because the strata slope down in the direction of the fault slip plane, and their thicknesses increase downward along the DF.

#### 4.2.2. Deformation of the footwall

As indicated by the bold arrow F (Fig. 4b), the strata showing a top-left shear sense below the fault plane are located between 6490 m (top of the DF) and 6960 m (interface of the BP\T). They exhibited nearly continuous parallel medium-strong seismic reflections, which are typical features of seismic reflections of rock assemblages in a ductile shear zone. This top-left, counterclockwise ductile shear deformation can be viewed through a microscope in the mylonite and phyllonite thin sections of the neighborhood well section (core samples 3 and 4, Fig. 3). Such changes in the intra-layer shear sense appear to be the result of friction coupled with relative motion in the rocks beneath the fault plane.

#### 4.2.3. Origin of the Early Cretaceous rifting center

The initial rifting center of the SLB is located at a large basement sag, which was originated from the interaction between the basement DF and the gravitational collapse of the hanging wall rocks, as well as the frictional drag action from the footwall rocks. This is a unique geological phenomenon, which we interpret as follows. Gravity causes the rock layer to collapse along the basement slip fault, and the frictional forces drag the rock strata upward. Under the combined action of the two forces, the Triassic basement strata on the hanging wall of the DF present a series of crescent-like structures that climb upward along the -gliding surface of the fault (crescents 1 and 2 in Fig. 4b). This indicates that the lower crescent body was formed stratigraphically earlier. The crescent-shaped deposit with the greatest curvature just below the ROU is located right in the center of the basin, where we drilled the borehole SK2. This depocenter survived for 39 million years (from 118 to 79 Ma) in the Cretaceous. Both the basin centers in the Early and Late Cretaceous are identified by the location of well SK2 (Fig. 2a and b), which is just above the TED of the basement rifting center (Figs. 4 and 5). This basin center lasted 16 Myrs from 118 to 102 Ma in the Early Cretaceous (see figure caption of Fig. 5). It lasted other 23 Myrs from 102 to 79 Ma in the late Early and Late Cretaceous, corresponding to the Denglouku to Nenjiang Formations (Fig. 1b). A comparison of basin centers between the Early and Late Cretaceous (Fig. 2a and b) shows that the center of the SLB showed no significant change in the location of Well SK2 from the Early to the Late Cretaceous (Fig. 2a and b). The time span in this case is from 118 to 79 Ma in the Cretaceous (see column C in Fig. 1b).

### 4.3. Rift onset unconformity (ROU)

As an indicator of basin startup, the ROU of the SLB was developed on top of the Triassic basement sequence and is recognized by a major uplift and erosional event preceded the rift phase, resulting in a widespread hiatus caused by erosion and peneplanation. In the following section, we describe the ROU in three dimensions: vertical sequence, profile features, and plane spread.

#### 4.3.1. Stratigraphic records of the rift onset unconformity

There is a regional unconformity developed between the Triassic basement and the overlying Cretaceous sedimentary cover (Fig. 3). The unconformity lies at a depth of 5960 m below the surface and is identified as the Cretaceous cover–Triassic basement boundary (BT\C, Fig. 3). The unconformity and its adjacent horizon above the Triassic basement recorded the initial rifting process of the basin. There was a long hiatus/interval of denudation of 124 Myr (242–118 Ma; column C of Fig. 3a) before the first cover of the Cretaceous volcanic ash deposit was formed. This event was revealed by two core samples near the BT\C. The lower sample, from a buried depth of 6032 m, is a Middle Triassic andesite dated to 242 Ma. Just above the BT\C (buried depth 5960 m), an Aptian tuff sample dated to 118 Ma was recovered. These observations from the SK2 borehole indicate that the upper Triassic and Jurassic formations are missing in the basin center. Another tuff core sample from 3961 m depth yielded an age of 114 Ma (Fig. 5). The sedimentation rate can thus be calculated as the depth difference of 1999 m divided by the time difference of 4 Myr resulting in 500 m/Myr (without correcting for compaction, same below). These initial four million years of rapid subsidence and deposition from 118 to 114 Ma were followed by slow and long-term basin subsidence from 114 to 102 Ma with a much slower sedimentation rate of 82 m/Myr. This event was revealed by a rhyolite core sample at a buried depth of 2972 m and yielded an age of 102 Ma (Fig. 5). The sedimentation rate can thus be calculated as (3961–2972) m/(114–102) Ma. These findings indicate that in the initial stage of basin formation, the SLB experienced a change from the long-term regional uplift and denudation to rapid subsidence and deposition, followed by long-term slow subsidence and deposition. Thus, basin dynamics underwent a transition from regional compression to fast extension and then to slow subsidence.

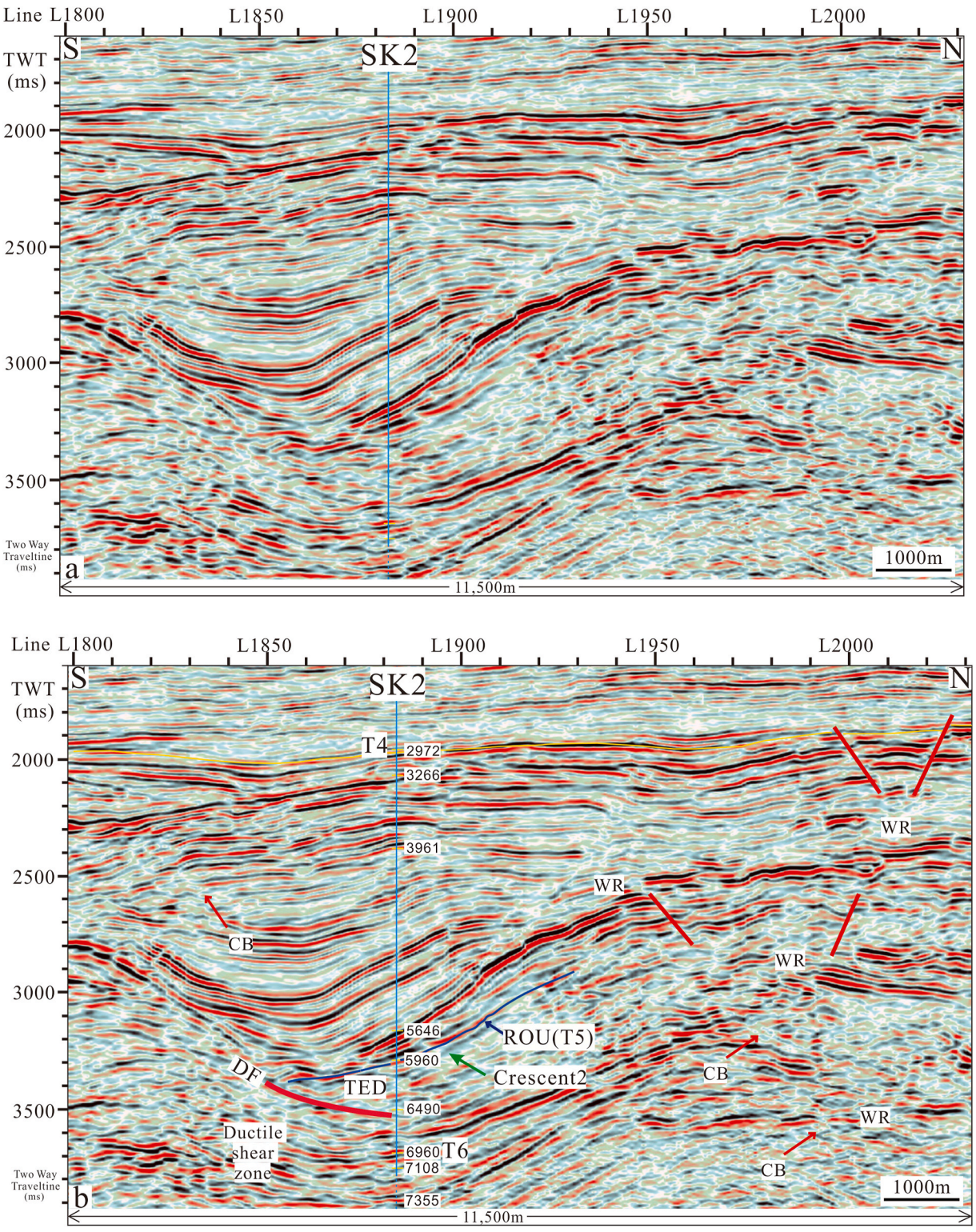


**Fig. 5.** Seismic profiles through the well SK2 from south to north. (a)- non-interpreted seismic profile and (b)- interpreted seismic section corresponding to a. It is a cross section perpendicular to that of Fig. 4 and the intersect is at the well SK2. The meanings of the symbols in the figure are the same as in Fig. 4.There are four sets of precise isotopic data with depth dating results of 5960 m (118 Ma), 3961 m (114 Ma), 3266 m (112 Ma), and 2972 m (102 Ma), which have been previously completed and published by our ICDP-SK2 geological group (Liu et al., 2021; Yu et al., 2020; Wang et al., 2022). See text for explanation about the sedimentation rates and corresponding basin filling patterns.

*4.3.2. Seismic profile of the rift onset unconformity and detachment fault*

Seismic profile through Well SK2 shows the relationship between DF, ROU, and overlying basin fills (Figs. 4 and 5). The lithology of Well SK2 at each depth section from 5900 to 7050 m is shown in Fig. 3. The ROU is at a depth of 5960 m, corresponding to the unconformity interface between the Cretaceous cover and Triassic basement, identified as BT\C in Fig. 3. The bottom of the Triassic sequence is at a depth of 6960 m, corresponding to the unconformity boundary between the Triassic and

Paleozoic successions, identified as BP\T in Fig. 3. The ROU was caused by lateral extension of the DF. When tracing the line of the ROU recognized as T5 in Fig. 4b, we can observe that the ROU is closely related to normal graben faults and forms lines between various fault points. This can be recognized by the fault points A, B, and C on the seismic profile (Fig. 4b), which correspond to the extensional and transtensional fault points A, B, and C on the plane contour map (Fig. 2b). The cross point between the ROU and DF (point A, Fig. 4b) indicates the starting point of the ROU, because this is the initial location where the post-orogenically thickened strata began to gravitatively slide along the fault plane. Thus, this location could be the cradle or starting point of the giant rift of the SLB. The thick high-angle red lines represent the graben faults, which are closely associated with intrusions. The intersection depth of the DF and Well SK2 is 6490 m, which is in the middle lower part of the kilometer-thick Triassic basement (530 m above and 470 m below).

#### 4.3.3. *Buried depth contour map of the rift onset unconformity*

The seismic reflection interface of T5-ROU developed in the region corresponds to the paleogeomorphology of the buried Triassic basement blocks and represents the boundary between the Cretaceous cover and Triassic basements of the BT\C at 5960 m well depth (Fig. 3). Because the kilometer-thick Triassic revealed by Well SK2 is the thickest Triassic strata discovered so far in the SLB and there is variation in the thickness of the Triassic, it can be inferred that the ROU will correspond to the BP \T interface where the Triassic is missing. A detailed mapping of the entire basin of the buried Triassic thickness on a large scale will provide further insights. Developed mainly on top of the Triassic basement sequence, the ROU is roughly equivalent to the bottom of the overlying Cretaceous basin fills. This shows that the accommodation space of an overlying basin is directly controlled by the syn-depositional uplift and subsidence of the underlying basement blocks, which are in turn controlled by the basement fault systems (Fig. 3).

### 4.4. *Overlying basin fills*

The seismic reflections correspond to the continuously cored Lower Cretaceous sections of 2988 m from a well depth of 5960–2972 m below the surface (Figs. 4 and 5). With the four sets of depth-dating results (5960 m-118 Ma; 3961 m-114 Ma; 3266 m-112 Ma; 2972 m-102 Ma), three episodes of sedimentation rate can thus be calculated by dividing the depth difference by the time difference (Fig. 5). They are 500 m/Myr (118–114 Ma, not corrected for compaction), 347 m/Myr (114–112 Ma), and 29 m/Myr (112–102 Ma). The average rate was 82 m/Myr during 114–102 Ma and that during 118–102 Ma was 187 m/Myr. Accordingly, three filling patterns corresponding to the above three phases can be recognized in the seismic profiles. They are as follows: (1) Large, thick lenticular sedimentary bodies with a collapsed shape at a buried depth of 5960–3961 m; (2) inclined thick-bedded vertical accretion fills at a depth of 3961–3266 m); (3) a horizontal, continuous, and steady vertical accretion sequence at a depth of 3266–2972 m (Fig. 4b and 5b).

## 5. Discussion

All the HMCC, HDF, and the SLB have shared a similar geological setting since the Jurassic because they were all developed on a “Pre-Triassic” basement system, called the united Heilongjiang Microplates (Wang et al., 2016). Therefore, the formation and evolution histories of the Jurassic–Cretaceous basins in these areas of Northeast Asia are comparable (Fig. 1a). We found crescent-shaped stratigraphic structures that migrated upwards along the gliding surface of the DF. This is due to the combination of the gravitational collapse of the hanging wall rocks and friction from the footwall rocks rather than a simple extension of the DF, as described by Ritts et al. (2010) in the HMCC and HDF region of Inner Mongolia of northeast China (Fig. 1a). In the case of the SLB, the hanging wall collapsed downward due to gravity along the gliding surface of the DF, and the footwall in the neighborhood dragged it upward due to friction. The combined action of the two forces resulted in sagging structures, which were formed sequentially from bottom to up along the low-angle plane of the DF. Both the downward curvature and size of these collapsed sags gradually increase when they climb upward along the gliding surface of the DF. The top, largest one was developed right above the ROU and at the center of the basin, where Well SK2 was drilled. Furthermore, the upward migration of the sags identified by the crescents 1 and 2 occurred only before the rift onset which is recognized by the ROU (T5). The bottom of the lower sag (Crescent 1) is at a depth about 6960 m, and that of the upper sag (Crescent 2) is at 5960 m, in which the upper sag combines with the ROU (T5), and they jointly form the rift onset unconformity indicating the initial rifting stage of the SLB in the Early Cretaceous in 118 Ma (Fig. 4b). After formation of the ROU, or, above the depth of 5960 m, there was little change in the basin center, which could last for up to 16 million years from 118 Ma to 102 Ma in the Early Cretaceous (Fig. 4b). It lasted for 39 Myr (118–79 Ma) in the Cretaceous (Fig. 1b). That can be recognized by comparing the basin center identified by the location of well SK2 in the Early and Late Cretaceous in Fig. 2a with b.

### 5.1. *Interaction between basement detachment fault, rift onset unconformity, and overlying basin fills*

#### 5.1.1. *Basement detachment fault and rift onset unconformity*

The SK2 borehole encountered a 618 m thick basement DF zone at a buried depth of 6490–7018 m (Fig. 4). Its top boundary (6490 m below the surface) was developed in the mid-lower part of the kilometer-thick Triassic basement sequence (530 m above and 470 m below). The interface between the Triassic and Paleozoic successions (BP\T, 6960 m, Fig. 3) is a brittle–ductile transition zone according to the deformation fabrics of the rocks above and below it, showing brittle deformation above and ductile deformation below the interface. The DF zone appears in the seismic profiles as shear, zonal, and nearly parallel medium-strong reflections (Figs. 4 and 5). A set of strong reflections located in the middle corresponds to the interface of the BP\T at 6960 m below the surface. The corresponding rocks are a set of metamorphic core complexes of mylonite and phyllonite (core samples 3 and 4; Fig. 3). The DF cut the ROU at a very low angle, and the extension of the DF caused a downward deflection of the basement sequence, which created the subsiding center of the basin (TED, Figs. 4 and 5). The brittle–ductile transition zone beneath the DF could be the most mobile and active factor during the interaction between the DF and ROU in the early rifting process of the SLB in the Early Cretaceous. This is because both the ductile fabric mylonite and phyllonite and the distinct strong seismic reflector in the ductile shear zone are observed at a depth of 6958–7035 m near the brittle–ductile transition zone (Figs. 3 and 4). The DF zone merges laterally in the Paleozoic strata at a burial depth below 7108 m, where its reflection features are less identifiable in the seismic profile (see the lower right in Fig. 4). As shown in the triangular region of fault point A, the ROU at a well depth of 5960 m, and the DF surface at 6490 m (Fig. 4b), the subsiding center of the SLB was created by the massive collapse of the hanging wall rocks along the gliding plane of the DF. This area represents the starting position of the ROU. This indicates that the giant rift of the SLB was initially ruptured from the triangular extensional domain (TED) and triggered by the extensional fault point A which was coupled with the ROU at 5960 m and the DF at 6490 m (see the triangular region in Figs. 4 and 5).

#### 5.1.2. *Triassic basement and Cretaceous sedimentary cover*

The basement lithologic sequence is composed of the Triassic and Late Paleozoic volcanic, igneous, pyroclastic, siliciclastic, and metamorphic rocks. It is a normal chronological sequence with a downward-aging succession (Fig. 3). The stratigraphic sequence of the basement seems nothing special compared with the cover layer. However, the upper most stratigraphic unit of the multi-layered basement successions

is particularly important in the following respects: First, the top interface is approximately equal to the bottom of the overlying sedimentary cover. In the case of the SLB, it is 1000 m of the Triassic volcanic and sedimentary successions, on top of which the ROU was developed. Present burial depth of the ROU is roughly equivalent to the stratigraphic thickness of the overlying Cretaceous basin fills (Fig. 3). Second, fault systems in the Triassic basement controlled the Early Cretaceous graben patterns and sediment distribution (Fig. 2). The basement faults cut the basement into blocks, and the inter-distributed Early Cretaceous sags and uplifts are bounded by these faults. Comparing basin centers recognized by the location of well SK2 in the Early and Late Cretaceous (Fig. 2a and b), it is observed that the basement fault systems must also have had a significant influence on the subsidence and sedimentation of the SLB in the Late Cretaceous, because the subsidence and depositional center of the basin was in the middle of the basement fault systems from the Early to Late Cretaceous, that is, near the location of Well SK2 borehole (see Fig. 2a and b). A significant basin-style transition occurred in the SLB from the separated fault grabens of the Lower Cretaceous to the unified large-sag basin of the Upper Cretaceous. The basin center of the latter continued until the tectonic inversion stage of the basin. This event is recognized by the Nenjiang orogenic movement recorded on top of the Nenjiang formation and occurred at about 79.1 Ma (Wang et al., 2016, Fig. 1b). Third, the Cenozoic reactivated Da'an–Dedu fault zone (DDFZ as described by Yu et al., 2018) is the main modern seismogenic structure in the region. It appears in the sedimentary cover and belongs to the western segment of the central fault systems at basement level (Fig. 2).

#### 5.1.3. Basement detachment fault and basin subsidence

This study indicates that basement DFs have a long-term controlling effect on the overlying basin fills. However, the controlling effect in the initial stage of basin development is significantly different from that in the later stages. The early rifting stage is characterized by a collapse-shaped thick lenticular deposit with an abnormally high sedimentation rate of up to 500 m/Myr (without compaction correction). This may correspond to a rapid breakup of the basement related to the ROU formation and hanging wall collapse associated with magmatic intrusions in the basement successions. The basin then experienced a long-term slow subsidence of the basement and aggradation of the basin filling pattern with a much lower sedimentation rate of 82 m/Myr, consisting of two phases with a declining sedimentary rate from 347 to 29 m/Myr. Generally, subsidence of the SLB results from the extension of the DF coupled with intrusive activities, as shown in Fig. 4 and described in Section 4.4. By analyzing the fault association in plane distribution (Fig. 2b) with corresponding vertical intrusive dykes (Fig. 4b) and comparing sedimentation rate with corresponding basin filling styles represented by the seismic profiles in Figs. 4 and 5, it is identified that there were three types of dynamic mechanisms leading to basement subsidence or uplift in the syn-rift stage of the SLB according to the time and space relationship between basement DF, volcanism and overlying basin fills. The first is extensional and/or transtensional faulting, as shown by the basement fault systems (Fig. 2b). A similar tectonic setting of the stress field was also indicated by the fragment component and facies analysis of the SK2 core section of 5690–5460 m (Fu et al., 2022). In addition, the SW-NE extension direction shown in the TED (Figs. 4 and 5) is consistent with the direction from the HDF (Davis et al., 2002) to the SK2 (Fig. 1a), which indicates that regional extensional faulting could have an influence on the initial rifting of the Songliao Basin. The second is gravitational collapse, as indicated by the collapse-shaped sedimentary bodies (Crescents 1, 2, Figs. 4 and 5). The third is upward magma flow, as shown by the feeder dykes coupled with high-angle normal faults of the grabens (Figs. 4 and 5). As mentioned above, the sedimentation rate of the SLB decreased continuously during the Early Cretaceous from 500 m/Myr (118–114 Ma) and 347 m/Myr (114–112 Ma) to 29 m/Myr (112–102 Ma); see section 4.4. The corresponding basin-filling patterns are large thick lenticular bodies (5960–3961 m), slanted intermittently layered deposits (3961–3266 m), and a horizontally continuous layered sequence (3266–2972 m; Figs. 4 and 5). How the three dynamic factors affect the quantitative process of basement uplift or subsidence of the SLB remains to be further studied. However, the main controlling factors of basin subsidence can be preliminarily summarized based on the spatial-temporal coupling between the DF, ROU, and overlying basin fills, as follows. The initial abnormally high subsidence can be attributed to the gravitational collapse resulting from the basement extension coupled with the magmatic intrusion. The last phase of the much slower subsidence appears to have been caused by regional thermal subsidence after the volcanic period. This intermediate factor may have been caused by the aforementioned combined factors.

#### 5.1.4. The effect of deep mantle flow on shallow accommodation space

Several sedimentary basins are known to be important archives of past mantle flow regimes. Mantle flow-induced dynamic topography may have a significant effect on the accommodation space in sedimentary basins (Xie et al., 2006; Vibe et al., 2018). However, the question remains: by what specific means does deep mantle flow influence the subsidence or uplift of a shallow basin? Fortunately, Well SK2 provides a good example of the response between a deep mantle flow and a shallow basin. The deep seismic profiles crossing Well SK2 revealed that deep mantle flow structures exist– at 60–70 km below the surface (Moho depth is 30 km), which are interpreted as early subduction relics (Fu et al., 2019). Note the special kind of oblique upward, intermittent medium-strong reflections identified by the bold marker WR in the seismic profiles (Figs. 4 and 5). They are worm- or snake-like in shape, moving upward and cutting through wall rocks. They are most likely the remnants of the upward migration of magma, known as feeder dykes, because they are closely associated with high-angle normal faults and cut and captured wall rock blocks (bold arrow CB, Fig. 4b and 5b). This conclusion is supported by the fine structure of the lithosphere beneath Well SK2 and the adjacent lithosphere, as revealed by the deep seismic reflection profiles. It was inferred that the upper mantle reflections beneath the SLB were likely resulted from the early subduction relics that could have subsequently become mantle-derived magma source (Fu et al., 2019) On the other hand, the magma upward flowing structures recognized by feeder dykes can be frequently observed at a buried depth of 7.355–2972 m in the seismic profiles (Figs. 4 and 5). The feeder dykes are closely associated with the high-angle normal faults of the rift grabens. As they move upward, they cut through all the underlying layers, including the basement and detachment faults. The feeder dykes coupled with the basement faults emerged at the interface of the ROU and shaped the morphology and tectonic pattern of the Early Cretaceous grabens (compare fault points A, B, and C in Fig. 2b and 4b). This cutting relationship indicates that the intrusions predated the ROU, i.e., before 118 Ma. The thermal effect caused by magma encroachment may be an important factor in the regional uplift; however, this is beyond the scope of this study. Therefore, it is reasonable to assume that mantle flow influences the overlying basin subsidence and/or uplift through the volume effect generated by the interaction between feeder dykes and basement fault systems during the upward migration of the related underlying magma.

### 5.2. Basin dynamics of the early rifting process in the Early Cretaceous

#### 5.2.1. Dynamics resulting in basin uplift and denudation

The Mesozoic–Cenozoic tectonic evolution of the SLB includes the following key geological events: the closure of the Paleo-Asian Ocean and Mongol–Okhotsk Ocean and the subduction of the Paleo-Pacific Ocean (Li et al., 2021). The closure of the eastern segment of the Paleo-Asian Ocean occurred during the Late Permian–Middle Triassic (Liu et al., 2017). Meanwhile, a kilometer-thick Middle Triassic basement volcano-sedimentary sequence was formed in the central SLB, as shown in Fig. 3. Subduction of the Paleo-Pacific Ocean had a definite influence on the dynamics and filling patterns of the SLB during the Late

Cretaceous recognized as an orogenic movement recorded on top of the Nenjiang formation (Fig. 1a; Feng et al., 2023). The lithospheric scale of tectonic evolution, ranging from the Siberian craton via the Mongol–Okhotsk suture zone to the SLB during the Kimmeridgian and the Aptian involved three pulsed stages: the southeastward subduction of the Mongol–Okhotsk oceanic crust that resulted in the suture between the Siberian craton and the Erguna-Xing'an-Songliao Blocks in the Kimmeridgian and Tithonian, the continental collision and lithospheric thickening in the Valanginian and the Hauterivian, and the post-collisional delamination of the thickened lithosphere and its extension during the Barremian up to the Aptian (Yu et al., 2022). Considering that the Upper Triassic and Jurassic volcanic sedimentary coal-bearing strata are widely distributed in the western SLB and Hailar Basin (unpublished), we interpret the record absence from 242 to 118 Ma (formation of the ROU) revealed by Well SK2 in the central SLB as being caused by differential uplift and denudation under the convergent tectonic setting related mainly to the Mongol–Okhotsk suturing event in the Late Jurassic and Early Cretaceous (Yang et al., 2015).

#### 5.2.2. *Dynamics resulting in the formation of the rift onset unconformity*

Determining the subsidence mechanism of a basin over a specific timeframe is usually difficult because vertical intraplate motions are not easily related to plate tectonics. Understanding the underlying mechanisms is further complicated by poor constraints on the magnitude and timing of these motions (Vibe et al., 2018).

Our results suggest that the DF in the basement is the primary factor controlling the subsidence of the overlying basin. Furthermore, sublithospheric mantle flow may affect the accommodation space of the overlying basin by cutting the basement block and shaping the graben pattern on top of the basement during the upward migration of the related underlying mantle-derived magma (Fu et al., 2019). The top part of the multi-layered basement sequence is composed of kilometer-thick Triassic strata that were cut by the DF of the basin through its middle lower part (530 m above and 470 m below; see section 4.2). The strata above the fault plane show a top-right clockwise rotation of deformation caused by gravitational collapse along the gliding surface of the fault. In contrast, the top-left counterclockwise rotational ductile deformations in the rocks below the fault plane can be observed in both core samples 3 and 4 and seismic reflections (Figs. 3 and 4). Such changes in the intra-layer shear sense appear to be the result of friction and relative motion in the rocks beneath the fault plane. A series of basement sags were formed under the combined action of the two forces. The largest one is located right in the center of the basin, where we drilled the borehole SK2. This depocenter survived for 39 million years, from 118 to 79 Ma (Figs. 1, 2 and 4). In the Late Cretaceous, significant changes occurred in the basin strike, structural style, and sedimentary sequence, but the basin center did not change significantly and remained in the SK2 position (compare Fig. 2a and b). To understand the reason for this, it requires further study. On the other hand, intrusive dykes played an important role in the segmentation of the basement block. This is similar to the case of the Norwegian–Greenland rift described by Gernigon et al. (2020). The intrusions are from deep mantle-derived magma source and recognized as a series of worm-like, upward or oblique, and zigzag seismic reflections (abbreviated as WR in Figs. 4 and 5). These events eventually led to the breaking of the basement blocks. In the seismic profiles, the extensional faults at the interface of the ROU correspond to the basement fault systems of the ROU in the corresponding contour map of the burial depth (see points A, B and C in Fig. 2b and 4b). This shows that the basement fault systems directly control the overlying sedimentary cover because the thicknesses of the strata above the basement blocks divided by these faults are significantly different from each other. Thus, we can define the ROU of an active continental margin volcanic rift as follows. After a long period of differential uplift and denudation, a DF was developed in the basement cutting the top stratigraphy of a multi-layered basement sequence vertically from the bottom to the top at a low angle. Subsequently, under the combined action of gravitational collapse, lateral extension, and magmatic intrusion, the basement assemblage was segmented into separate blocks, followed by the first phase of rapid basement subsidence. Finally, the first sedimentary cover was formed, which commonly consisted of volcanic ash or tuffaceous deposits.

## 6. Conclusion

Under the thick Cretaceous sedimentary cover, a multi-layered basement succession with a downward aging sequence composed of the Triassic and Paleozoic deposits was developed in the Songliao Basin (SLB). A similar downward-aging basement sequence is expected in the deeper part of the basin. The basement of a sedimentary basin is the first basement structural sequence beneath the main sedimentary cover of interest. The Triassic of the SLB is of great importance for the overlying Cretaceous basin fills. Because the BT\C boundary between the Triassic basement and Cretaceous cover experienced and recorded the process and results of the interaction between the underlying basement and the sedimentary cover (Fig. 3a). The rift onset unconformity (ROU) was developed on top of the Triassic basement, which is characterized by a long-term hiatus/interval of denudation of 124 Myr (242–118 Ma). The first layer of volcanic ash deposits marks the beginning of basin formation during the Cretaceous. The features of long-term denudation and volcanic ash deposition may be common to the ROU in a volcanic rift basin. The orientation of the triangular extentional domain (TED) beneath the rift onset unconformity (ROU) and above the basement detachment fault (DF) in the basement strata. is consistent with the SW-NE striking of the regional extensional decollement in northeastern China (Fig. 1a). Resulted from interaction between the ROU, DF and magmatic intrusion, the TED marks the location of the initial rupture of the SLB. The center of the basin is situated in the largest depression at the ROU interface which is closely associated to the TED. The DF cuts the kilometer-thick Triassic basement sequence in its middle lower part with a low-angle fault-gliding surface along which the hanging wall collapsed because of gravity. This resulted in a series of sagging structures climbing upward. The top greatest sag was developed right above the ROU and was located right in the center of the basin, which survived for 39 Myr from 118 to 79 Ma in the Cretaceous. The combination of DF and volcanism is the primary controlling factor for basin subsidence in the early rifting process of 16 Myr during the syn-rift stage from 118 to 102 Ma. Gravitational collapse produced the maximum sedimentation rate of 500 m/Myr from 118 to 114 Ma, which was caused by extension of the DF. The long-term thermal subsidence following the volcanic period resulted in a minimal sedimentation rate of 29 m/Myr (112-102 Ma). In the transition stage of the two subsiding mechanisms, an intermediate sedimentation rate of 347 m/Myr appeared in the middle syn-rift stage from 114 to 112 Ma. The center of the SLB sits on a system of long-active volcanic conduits that were active intermittently from 242 to 102 Ma in the basement successions. A set of deep mantle flow structures exists 60–70 km below the surface at the center of the basin. Sublithospheric mantle flow may affect the accommodation space of the overlying basin by feeder dykes' cutting the basement blocks and shaping the graben pattern on top of the basement during the upward migration of the related underlying mantle-derived magma. The intrusions might have triggered basement extension, leading to the formation of the ROU and subsequently causing thermal subsidence in the evolution period of the basin.

**Table 1**
LA-ICP-MS zircon U-Pb dating data for the samples of SK-2.

| Sample | Sample No. | Th (ppm) | U (ppm) | Th/U | U-Th-Pb isotope ratio | | | | | | Age (Ma) | | | | | |
|---|---|---|---|---|---|---|---|---|---|---|---|---|---|---|---|---|
| | | | | | $^{207}Pb/^{206}Pb$ | $^{207}Pb/^{206}Pb$ | $^{207}Pb/^{235}U$ | $^{207}Pb/^{235}U$ | $^{206}Pb/^{238}U$ | $^{206}Pb/^{238}U$ | $^{207}Pb/^{206}Pb$ | $^{207}Pb/^{206}Pb$ | $^{207}Pb/^{235}U$ | $^{207}Pb/^{235}U$ | $^{206}Pb/^{238}U$ | $^{206}Pb/^{238}U$ |
| | | | | | Ratio | 1σ | Ratio | 1σ | Ratio | 1σ | Age | 1σ | Age | 1σ | Age | 1σ |
| ①6453.17m Andesite | S2-34-01 | 83 | 159 | 0.52 | 0.09492 | 0.00240 | 2.02046 | 0.04726 | 0.15432 | 0.00154 | 1527 | 47 | 1122 | 16 | 925 | 9 |
| | S2-34-02 | 296 | 299 | 0.99 | 0.05481 | 0.00208 | 0.30056 | 0.01085 | 0.03976 | 0.00041 | 404 | 82 | 267 | 8 | 251 | 3 |
| | S2-34-03 | 112 | 237 | 0.47 | 0.07063 | 0.00197 | 1.50848 | 0.03955 | 0.15484 | 0.00152 | 947 | 56 | 934 | 16 | 928 | 9 |
| | S2-34-04 | 225 | 241 | 0.94 | 0.06226 | 0.00306 | 0.32303 | 0.01527 | 0.03762 | 0.00050 | 683 | 102 | 284 | 12 | 238 | 3 |
| | S2-34-05 | 248 | 502 | 0.49 | 0.05503 | 0.00282 | 0.29954 | 0.01480 | 0.03947 | 0.00052 | 413 | 110 | 266 | 12 | 250 | 3 |
| | S2-34-06 | 243 | 251 | 0.97 | 0.05347 | 0.00219 | 0.28324 | 0.01109 | 0.03841 | 0.00041 | 349 | 90 | 253 | 9 | 243 | 3 |
| | S2-34-07 | 138 | 148 | 0.94 | 0.05386 | 0.00562 | 0.28561 | 0.02909 | 0.03845 | 0.00097 | 365 | 220 | 255 | 23 | 243 | 6 |
| | S2-34-08 | 73 | 98 | 0.75 | 0.05519 | 0.00313 | 0.31130 | 0.01711 | 0.04090 | 0.00058 | 420 | 121 | 275 | 13 | 258 | 4 |
| | S2-34-09 | 114 | 155 | 0.73 | 0.05166 | 0.00496 | 0.27990 | 0.02621 | 0.03929 | 0.00089 | 270 | 206 | 251 | 21 | 248 | 6 |
| | S2-34-10 | 77 | 135 | 0.57 | 0.05366 | 0.00348 | 0.28926 | 0.01820 | 0.03909 | 0.00063 | 357 | 140 | 258 | 14 | 247 | 4 |
| | S2-34-11 | 101 | 122 | 0.83 | 0.05154 | 0.00724 | 0.27943 | 0.03837 | 0.03932 | 0.00129 | 265 | 294 | 250 | 30 | 249 | 8 |
| | S2-34-12 | 167 | 168 | 0.99 | 0.05218 | 0.00336 | 0.27662 | 0.01729 | 0.03844 | 0.00060 | 293 | 140 | 248 | 14 | 243 | 4 |
| | S2-34-13 | 258 | 263 | 0.98 | 0.05224 | 0.00290 | 0.27501 | 0.01476 | 0.03818 | 0.00053 | 296 | 122 | 247 | 12 | 242 | 3 |
| | S2-34-14 | 119 | 134 | 0.89 | 0.05051 | 0.00504 | 0.27519 | 0.02682 | 0.03951 | 0.00093 | 219 | 216 | 247 | 21 | 250 | 6 |
| | S2-34-15 | 40 | 73 | 0.54 | 0.05280 | 0.00380 | 0.28082 | 0.01965 | 0.03857 | 0.00067 | 320 | 155 | 251 | 16 | 244 | 4 |
| | S2-34-16 | 229 | 224 | 1.02 | 0.05235 | 0.00546 | 0.28055 | 0.02853 | 0.03887 | 0.00097 | 301 | 222 | 251 | 23 | 246 | 6 |
| | S2-34-17 | 123 | 170 | 0.72 | 0.05183 | 0.00322 | 0.27596 | 0.01662 | 0.03862 | 0.00059 | 278 | 136 | 248 | 13 | 244 | 4 |
| | S2-34-18 | 308 | 335 | 0.92 | 0.05326 | 0.00216 | 0.28118 | 0.01092 | 0.03829 | 0.00041 | 340 | 89 | 252 | 9 | 242 | 3 |
| | S2-34-19 | 293 | 196 | 1.50 | 0.05150 | 0.00304 | 0.27335 | 0.01567 | 0.03849 | 0.00056 | 263 | 130 | 245 | 12 | 244 | 3 |
| | S2-34-20 | 105 | 158 | 0.66 | 0.05237 | 0.00469 | 0.27478 | 0.02398 | 0.03805 | 0.00082 | 302 | 192 | 247 | 19 | 241 | 5 |
| | S2-34-21 | 512 | 326 | 1.57 | 0.05089 | 0.00277 | 0.26962 | 0.01422 | 0.03843 | 0.00052 | 236 | 121 | 242 | 11 | 243 | 3 |
| | S2-34-22 | 166 | 175 | 0.95 | 0.05249 | 0.00324 | 0.27731 | 0.01659 | 0.03831 | 0.00059 | 307 | 134 | 249 | 13 | 242 | 4 |
| | S2-34-23 | 328 | 263 | 1.25 | 0.05216 | 0.00196 | 0.27513 | 0.00987 | 0.03826 | 0.00038 | 292 | 83 | 247 | 8 | 242 | 2 |
| | S2-34-24 | 82 | 101 | 0.81 | 0.05218 | 0.00300 | 0.27900 | 0.01555 | 0.03878 | 0.00055 | 293 | 126 | 250 | 12 | 245 | 3 |
| | S2-34-25 | 180 | 216 | 0.83 | 0.05138 | 0.00257 | 0.27143 | 0.01310 | 0.03832 | 0.00048 | 258 | 111 | 244 | 10 | 242 | 3 |

(*continued on next page*)

**Table 1** (*continued*)

| Sample | Sample No. | Th (ppm) | U (ppm) | Th/U | U-Th-Pb isotope ratio | | | | | | Age (Ma) | | | | | |
|---|---|---|---|---|---|---|---|---|---|---|---|---|---|---|---|---|
| | | | | | $^{207}Pb/^{206}Pb$ | $^{207}Pb/^{206}Pb$ | $^{207}Pb/^{235}U$ | $^{207}Pb/^{235}U$ | $^{206}Pb/^{238}U$ | $^{206}Pb/^{238}U$ | $^{207}Pb/^{206}Pb$ | $^{207}Pb/^{206}Pb$ | $^{207}Pb/^{235}U$ | $^{207}Pb/^{235}U$ | $^{206}Pb/^{238}U$ | $^{206}Pb/^{238}U$ |
| | | | | | Ratio | 1σ | Ratio | 1σ | Ratio | 1σ | Age | 1σ | Age | 1σ | Age | 1σ |
| | S2-34-26 | 783 | 571 | 1.37 | 0.05306 | 0.00221 | 0.27990 | 0.01120 | 0.03826 | 0.00042 | 331 | 92 | 251 | 9 | 242 | 3 |
| | S2-34-27 | 54 | 86 | 0.63 | 0.05054 | 0.00306 | 0.26756 | 0.01575 | 0.03839 | 0.00054 | 220 | 134 | 241 | 13 | 243 | 3 |
| | S2-34-28 | 166 | 202 | 0.82 | 0.05089 | 0.00286 | 0.27992 | 0.01525 | 0.03989 | 0.00056 | 236 | 125 | 251 | 12 | 252 | 3 |
| | S2-34-29 | 162 | 584 | 0.28 | 0.07019 | 0.00087 | 1.50167 | 0.01354 | 0.15514 | 0.00090 | 934 | 25 | 931 | 6 | 930 | 5 |
| | S2-34-30 | 929 | 442 | 2.10 | 0.05045 | 0.00191 | 0.26857 | 0.00971 | 0.03861 | 0.00039 | 216 | 85 | 242 | 8 | 244 | 2 |
| ②6958.38m Granite porphyry | S3-43-1 | 1114 | 987 | 1.13 | 0.05447 | 0.00332 | 0.28687 | 0.03836 | 0.03746 | 0.00150 | 391 | 132 | 256 | 15 | 237 | 5 |
| | S3-43-2 | 1362 | 1139 | 1.20 | 0.05511 | 0.00421 | 0.30204 | 0.04794 | 0.03925 | 0.00278 | 417 | 177 | 268 | 19 | 248 | 9 |
| | S3-43-3 | 353 | 373 | 0.95 | 0.10324 | 0.01256 | 0.56301 | 0.13403 | 0.03959 | 0.00287 | 1683 | 226 | 453 | 44 | 250 | 9 |
| | S3-43-4 | 279 | 273 | 1.02 | 0.04863 | 0.00630 | 0.25926 | 0.06932 | 0.03794 | 0.00182 | 132 | 278 | 234 | 28 | 240 | 6 |
| | S3-43-5 | 1375 | 1032 | 1.33 | 0.05834 | 0.00390 | 0.26329 | 0.03195 | 0.03264 | 0.00140 | 543 | 146 | 237 | 13 | 207 | 4 |
| | S3-43-6 | 573 | 612 | 0.94 | 0.10377 | 0.02585 | 0.66993 | 0.44899 | 0.03781 | 0.00254 | 1692 | 474 | 521 | 137 | 239 | 8 |
| | S3-43-7 | 538 | 437 | 1.23 | 0.06154 | 0.00713 | 0.31863 | 0.08195 | 0.03622 | 0.00161 | 657 | 251 | 281 | 32 | 229 | 5 |
| | S3-43-8 | 867 | 919 | 0.94 | 0.07785 | 0.00787 | 0.39825 | 0.06940 | 0.03731 | 0.00202 | 1143 | 202 | 340 | 25 | 236 | 6 |
| | S3-43-9 | 522 | 491 | 1.06 | 0.05219 | 0.00338 | 0.27912 | 0.03231 | 0.03892 | 0.00111 | 295 | 148 | 250 | 13 | 246 | 3 |
| | S3-43-10 | 309 | 291 | 1.06 | 0.08840 | 0.01021 | 0.44892 | 0.11421 | 0.03574 | 0.00122 | 1391 | 223 | 377 | 40 | 226 | 4 |
| | S3-43-11 | 1094 | 904 | 1.21 | 0.05108 | 0.00226 | 0.27757 | 0.02605 | 0.03896 | 0.00130 | 243 | 102 | 249 | 10 | 246 | 4 |
| | S3-43-12 | 332 | 352 | 0.94 | 0.05788 | 0.00424 | 0.31204 | 0.04360 | 0.03947 | 0.00203 | 524 | 156 | 276 | 17 | 250 | 6 |
| | S3-43-13 | 1137 | 879 | 1.29 | 0.10734 | 0.01040 | 0.56591 | 0.13777 | 0.03767 | 0.00462 | 1755 | 179 | 455 | 45 | 238 | 14 |
| | S3-43-14 | 265 | 290 | 0.91 | 0.05585 | 0.00481 | 0.29671 | 0.04696 | 0.03875 | 0.00168 | 456 | 193 | 264 | 18 | 245 | 5 |
| | S3-43-15 | 884 | 829 | 1.07 | 0.05573 | 0.00317 | 0.29337 | 0.03697 | 0.03816 | 0.00221 | 443 | 128 | 261 | 15 | 241 | 7 |
| | S3-43-16 | 1073 | 975 | 1.10 | 0.05761 | 0.00289 | 0.28899 | 0.02771 | 0.03619 | 0.00104 | 517 | 77 | 258 | 11 | 229 | 3 |
| | S3-43-17 | 806 | 718 | 1.12 | 0.05585 | 0.00420 | 0.29837 | 0.04314 | 0.03861 | 0.00140 | 456 | 136 | 265 | 17 | 244 | 4 |
| | S3-43-18 | 724 | 433 | 1.67 | 0.05546 | 0.00443 | 0.29172 | 0.04618 | 0.03793 | 0.00116 | 432 | 178 | 260 | 18 | 240 | 4 |
| | S3-43-19 | 416 | 394 | 1.06 | 0.10395 | 0.00940 | 0.62523 | 0.12271 | 0.04303 | 0.00271 | 1696 | 167 | 493 | 38 | 272 | 8 |
| | S3-43-20 | 1319 | 1019 | 1.29 | 0.07202 | 0.01027 | 0.36324 | 0.11085 | 0.03594 | 0.00123 | 987 | 294 | 315 | 41 | 228 | 4 |
| | S3-43-21 | 428 | 424 | 1.01 | 0.05642 | 0.00356 | 0.30205 | 0.03459 | 0.03877 | 0.00182 | 478 | 144 | 268 | 13 | 245 | 6 |
| | S3-43-22 | 2186 | 1466 | 1.49 | 0.05398 | 0.00253 | 0.28577 | 0.02912 | 0.03804 | 0.00161 | 369 | 106 | 255 | 12 | 241 | 5 |
| | S3-43-23 | 702 | 598 | 1.17 | 0.07841 | 0.00699 | 0.42444 | 0.08400 | 0.03918 | 0.00288 | 1167 | 178 | 359 | 30 | 248 | 9 |
| | S3-43-24 | 1103 | 914 | 1.21 | 0.05725 | 0.00266 | 0.30603 | 0.02616 | 0.03902 | 0.00112 | 502 | 108 | 271 | 10 | 247 | 3 |
| | S3-43-25 | 1666 | 1281 | 1.30 | 0.06743 | 0.00454 | 0.32579 | 0.04924 | 0.03397 | 0.00112 | 850 | 141 | 286 | 19 | 215 | 3 |

(*continued on next page*)

**Table 1** (*continued*)

| Sample | Sample No. | Th (ppm) | U (ppm) | Th/U | U-Th-Pb isotope ratio | | | | | | Age (Ma) | | | | | |
|---|---|---|---|---|---|---|---|---|---|---|---|---|---|---|---|---|
| | | | | | $^{207}Pb/^{206}Pb$ | $^{207}Pb/^{206}Pb$ | $^{207}Pb/^{235}U$ | $^{207}Pb/^{235}U$ | $^{206}Pb/^{238}U$ | $^{206}Pb/^{238}U$ | $^{207}Pb/^{206}Pb$ | $^{207}Pb/^{206}Pb$ | $^{207}Pb/^{235}U$ | $^{207}Pb/^{235}U$ | $^{206}Pb/^{238}U$ | $^{206}Pb/^{238}U$ |
| | | | | | Ratio | 1σ | Ratio | 1σ | Ratio | 1σ | Age | 1σ | Age | 1σ | Age | 1σ |
| | S3-43-26 | 1071 | 930 | 1.15 | 0.07837 | 0.00535 | 0.41110 | 0.06293 | 0.03734 | 0.00129 | 1167 | 136 | 350 | 23 | 236 | 4 |
| | S3-43-27 | 806 | 689 | 1.17 | 0.06385 | 0.00326 | 0.31367 | 0.03135 | 0.03559 | 0.00115 | 744 | 105 | 277 | 12 | 225 | 4 |
| | S3-43-28 | 667 | 635 | 1.05 | 0.06773 | 0.00436 | 0.36273 | 0.04566 | 0.03869 | 0.00138 | 861 | 134 | 314 | 17 | 245 | 4 |
| | S3-43-29 | 903 | 766 | 1.18 | 0.06474 | 0.00603 | 0.34621 | 0.07042 | 0.03791 | 0.00126 | 765 | 192 | 302 | 27 | 240 | 4 |
| | S3-43-30 | 2366 | 1504 | 1.57 | 0.05593 | 0.00426 | 0.28112 | 0.03749 | 0.03812 | 0.00680 | 450 | 138 | 252 | 15 | 241 | 21 |
| ③6973.10m Mylonite | S3-46-1 | 92 | 329 | 0.28 | 0.05713 | 0.00513 | 0.28452 | 0.02463 | 0.03647 | 0.00090 | 498 | 198 | 254 | 19 | 231 | 6 |
| | S3-46-2 | 838 | 1457 | 0.58 | 0.05743 | 0.00792 | 0.29046 | 0.04132 | 0.03704 | 0.00192 | 509 | 307 | 259 | 33 | 234 | 12 |
| | S3-46-3 | 423 | 553 | 0.77 | 0.07715 | 0.01168 | 0.46329 | 0.06001 | 0.04571 | 0.00118 | 1125 | 310 | 387 | 42 | 288 | 7 |
| | S3-46-4 | 627 | 836 | 0.75 | 0.04195 | 0.00971 | 0.26285 | 0.06648 | 0.04123 | 0.00147 | error | | 237 | 53 | 260 | 9 |
| | S3-46-5 | 1049 | 1158 | 0.91 | 0.07617 | 0.00384 | 1.43766 | 0.07208 | 0.13651 | 0.00391 | 1100 | 102 | 905 | 30 | 825 | 22 |
| | S3-46-6 | 416 | 670 | 0.62 | 0.26109 | 0.01874 | 2.17159 | 0.18428 | 0.05751 | 0.00204 | 3253 | 113 | 1172 | 59 | 360 | 12 |
| | S3-46-7 | 276 | 466 | 0.59 | 0.05485 | 0.00247 | 0.31165 | 0.01438 | 0.04068 | 0.00073 | 406 | 102 | 275 | 11 | 257 | 5 |
| | S3-46-8 | 171 | 491 | 0.35 | 0.09827 | 0.01326 | 0.61842 | 0.08830 | 0.04385 | 0.00183 | 1592 | 254 | 489 | 55 | 277 | 11 |
| | S3-46-9 | 139 | 275 | 0.51 | 0.05751 | 0.00573 | 0.34674 | 0.03243 | 0.04362 | 0.00089 | 509 | 220 | 302 | 24 | 275 | 6 |
| | S3-46-10 | 173 | 380 | 0.46 | 0.11217 | 0.01111 | 0.68235 | 0.06613 | 0.04354 | 0.00116 | 1835 | 181 | 528 | 40 | 275 | 7 |
| | S3-46-11 | 396 | 526 | 0.75 | 0.15368 | 0.01828 | 1.34064 | 0.23255 | 0.05299 | 0.00379 | 2387 | 204 | 864 | 101 | 333 | 23 |
| | S3-46-12 | 904 | 789 | 1.15 | 0.18760 | 0.02726 | 0.79935 | 0.09624 | 0.03939 | 0.00205 | 2721 | 241 | 596 | 54 | 249 | 13 |
| | S3-46-13 | 1740 | 4205 | 0.41 | 0.07119 | 0.00747 | 0.45019 | 0.04798 | 0.04793 | 0.00138 | 963 | 217 | 377 | 34 | 302 | 8 |
| | S3-46-14 | 471 | 819 | 0.58 | 0.07317 | 0.00900 | 0.46980 | 0.05532 | 0.04446 | 0.00126 | 1020 | 252 | 391 | 38 | 280 | 8 |
| | S3-46-15 | 1035 | 2927 | 0.35 | 0.04841 | 0.00307 | 0.28124 | 0.01776 | 0.04172 | 0.00071 | 120 | 141 | 252 | 14 | 263 | 4 |
| | S3-46-16 | 391 | 867 | 0.45 | 0.07317 | 0.00673 | 0.45361 | 0.03906 | 0.04453 | 0.00095 | 1020 | 187 | 380 | 27 | 281 | 6 |
| | S3-46-17 | 656 | 1627 | 0.40 | 0.17465 | 0.00477 | 19.40214 | 1.56229 | 0.78214 | 0.05263 | 2603 | 40 | 3062 | 78 | 3725 | 190 |
| | S3-46-18 | 525 | 1311 | 0.40 | 0.05859 | 0.00347 | 0.34659 | 0.01897 | 0.04341 | 0.00068 | 554 | 130 | 302 | 14 | 274 | 4 |
| | S3-46-19 | 538 | 1344 | 0.40 | 0.05803 | 0.00303 | 0.34949 | 0.01768 | 0.04371 | 0.00069 | 532 | 115 | 304 | 13 | 276 | 4 |
| | S3-46-20 | 643 | 842 | 0.76 | 0.10283 | 0.01128 | 0.65054 | 0.07309 | 0.04577 | 0.00131 | 1676 | 204 | 509 | 45 | 288 | 8 |
| | S3-46-21 | 281 | 646 | 0.44 | 0.05573 | 0.00370 | 0.31782 | 0.02321 | 0.04126 | 0.00174 | 443 | 148 | 280 | 18 | 261 | 11 |
| | S3-46-22 | 746 | 717 | 1.04 | 0.05775 | 0.00229 | 0.63840 | 0.02557 | 0.07972 | 0.00106 | 520 | 87 | 501 | 16 | 494 | 6 |
| | S3-46-23 | 905 | 2762 | 0.33 | 0.05724 | 0.00559 | 0.33911 | 0.02965 | 0.04308 | 0.00083 | 502 | 184 | 296 | 22 | 272 | 5 |
| | S3-46-24 | 737 | 939 | 0.78 | 0.06597 | 0.00672 | 0.38082 | 0.03692 | 0.04265 | 0.00127 | 806 | 215 | 328 | 27 | 269 | 8 |
| | S3-46-25 | 290 | 710 | 0.41 | 0.08742 | 0.00593 | 0.57994 | 0.04201 | 0.04830 | 0.00144 | 1369 | 131 | 464 | 27 | 304 | 9 |

(*continued on next page*)

**Table 1** (*continued*)

| Sample | Sample No. | Th (ppm) | U (ppm) | Th/U | U-Th-Pb isotope ratio | | | | | | Age (Ma) | | | | | |
|---|---|---|---|---|---|---|---|---|---|---|---|---|---|---|---|---|
| | | | | | $^{207}Pb/^{206}Pb$ | $^{207}Pb/^{206}Pb$ | $^{207}Pb/^{235}U$ | $^{207}Pb/^{235}U$ | $^{206}Pb/^{238}U$ | $^{206}Pb/^{238}U$ | $^{207}Pb/^{206}Pb$ | $^{207}Pb/^{206}Pb$ | $^{207}Pb/^{235}U$ | $^{207}Pb/^{235}U$ | $^{206}Pb/^{238}U$ | $^{206}Pb/^{238}U$ |
| | | | | | Ratio | 1σ | Ratio | 1σ | Ratio | 1σ | Age | 1σ | Age | 1σ | Age | 1σ |
| | S3-46-26 | 908 | 3325 | 0.27 | 0.06484 | 0.00341 | 0.38165 | 0.02134 | 0.04193 | 0.00053 | 769 | 111 | 328 | 16 | 265 | 3 |
| | S3-46-27 | 1391 | 1688 | 0.82 | 0.07583 | 0.00594 | 1.07902 | 0.09057 | 0.10319 | 0.00414 | 1100 | 158 | 743 | 44 | 633 | 24 |
| | S3-46-28 | 772 | 1391 | 0.56 | 0.05357 | 0.00634 | 0.30388 | 0.03496 | 0.04095 | 0.00094 | 354 | 275 | 269 | 27 | 259 | 6 |
| | S3-46-29 | 813 | 1371 | 0.59 | 0.05562 | 0.00578 | 0.29516 | 0.02730 | 0.03955 | 0.00107 | 439 | 233 | 263 | 21 | 250 | 7 |
| | S3-46-30 | 1363 | 1457 | 0.94 | 0.09698 | 0.00990 | 0.53886 | 0.05068 | 0.04055 | 0.00105 | 1569 | 192 | 438 | 33 | 256 | 7 |
| ④7035.00m Phyllonite | S3-51-1 | 421 | 857 | 0.49 | 0.08238 | 0.00266 | 0.79512 | 0.02502 | 0.07089 | 0.00108 | 1255 | 63 | 594 | 14 | 442 | 6 |
| | S3-51-2 | 572 | 1072 | 0.53 | 0.06841 | 0.00802 | 0.49710 | 0.02698 | 0.05628 | 0.00070 | 881 | 245 | 410 | 18 | 353 | 4 |
| | S3-51-3 | 384 | 798 | 0.48 | 0.06124 | 0.00188 | 0.54775 | 0.01654 | 0.06494 | 0.00077 | 656 | 67 | 444 | 11 | 406 | 5 |
| | S3-51-4 | 387 | 795 | 0.49 | 0.06015 | 0.00254 | 0.47407 | 0.01912 | 0.05778 | 0.00080 | 609 | 88 | 394 | 13 | 362 | 5 |
| | S3-51-5 | 432 | 861 | 0.50 | 0.05745 | 0.00224 | 0.46850 | 0.01792 | 0.05906 | 0.00069 | 509 | 85 | 390 | 12 | 370 | 4 |
| | S3-51-6 | 485 | 926 | 0.52 | 0.07933 | 0.00400 | 0.65500 | 0.03495 | 0.05935 | 0.00092 | 1181 | 100 | 512 | 21 | 372 | 6 |
| | S3-51-7 | 361 | 806 | 0.45 | 0.07200 | 0.00449 | 0.57127 | 0.03785 | 0.05698 | 0.00077 | 987 | 128 | 459 | 24 | 357 | 5 |
| | S3-51-8 | 649 | 845 | 0.77 | 0.11207 | 0.00753 | 0.91996 | 0.08001 | 0.05602 | 0.00106 | 1833 | 122 | 662 | 42 | 351 | 7 |
| | S3-51-9 | 472 | 923 | 0.51 | 0.06026 | 0.00286 | 0.49117 | 0.02383 | 0.05897 | 0.00084 | 613 | 108 | 406 | 16 | 369 | 5 |
| | S3-51-10 | 439 | 867 | 0.51 | 0.07463 | 0.00313 | 0.64061 | 0.02878 | 0.06169 | 0.00084 | 1058 | 84 | 503 | 18 | 386 | 5 |
| | S3-51-11 | 697 | 1228 | 0.57 | 0.05751 | 0.00170 | 0.49168 | 0.01475 | 0.06168 | 0.00061 | 522 | 60 | 406 | 10 | 386 | 4 |
| | S3-51-12 | 875 | 1324 | 0.66 | 0.07725 | 0.01132 | 0.61927 | 0.08711 | 0.05817 | 0.00091 | 1128 | 295 | 489 | 55 | 365 | 6 |
| | S3-51-13 | 326 | 572 | 0.57 | 0.06022 | 0.00205 | 0.82622 | 0.02794 | 0.09910 | 0.00101 | 613 | 42 | 612 | 16 | 609 | 6 |
| | S3-51-14 | 381 | 777 | 0.49 | 0.05855 | 0.00243 | 0.51388 | 0.02230 | 0.06327 | 0.00072 | 550 | 91 | 421 | 15 | 395 | 4 |
| | S3-51-15 | 461 | 882 | 0.52 | 0.05887 | 0.00183 | 0.50918 | 0.01525 | 0.06252 | 0.00061 | 561 | 67 | 418 | 10 | 391 | 4 |
| | S3-51-16 | 390 | 815 | 0.48 | 0.05323 | 0.00208 | 0.46137 | 0.01776 | 0.06258 | 0.00064 | 339 | 89 | 385 | 12 | 391 | 4 |
| | S3-51-17 | 1808 | 1563 | 1.16 | 0.05518 | 0.00167 | 0.46501 | 0.01390 | 0.06084 | 0.00067 | 420 | 69 | 388 | 10 | 381 | 4 |
| | S3-51-18 | 592 | 1130 | 0.52 | 0.05899 | 0.00270 | 0.45109 | 0.02054 | 0.05533 | 0.00088 | 565 | 100 | 378 | 14 | 347 | 5 |
| | S3-51-19 | 992 | 1516 | 0.65 | 0.06858 | 0.00151 | 1.42233 | 0.03207 | 0.14908 | 0.00158 | 887 | 46 | 898 | 13 | 896 | 9 |
| | S3-51-20 | 587 | 1086 | 0.54 | 0.05632 | 0.00180 | 0.48640 | 0.01557 | 0.06225 | 0.00065 | 465 | 105 | 402 | 11 | 389 | 4 |
| | S3-51-21 | 545 | 1009 | 0.54 | 0.05612 | 0.00199 | 0.46986 | 0.01527 | 0.06100 | 0.00068 | 457 | 112 | 391 | 11 | 382 | 4 |
| | S3-51-22 | 668 | 1190 | 0.56 | 0.05707 | 0.00181 | 0.47382 | 0.01495 | 0.06009 | 0.00074 | 494 | 64 | 394 | 10 | 376 | 5 |
| | S3-51-23 | 463 | 926 | 0.50 | 0.05602 | 0.00186 | 0.44563 | 0.01468 | 0.05764 | 0.00072 | 454 | 74 | 374 | 10 | 361 | 4 |
| | S3-51-24 | 758 | 974 | 0.78 | 0.05210 | 0.00166 | 0.44166 | 0.01407 | 0.06121 | 0.00066 | 300 | 72 | 371 | 10 | 383 | 4 |
| | S3-51-25 | 479 | 950 | 0.50 | 0.06101 | 0.00217 | 0.51428 | 0.01743 | 0.06129 | 0.00080 | 639 | 81 | 421 | 12 | 383 | 5 |

## CRediT authorship contribution statement

**Pujun Wang:** Writing – original draft, Project administration, Methodology. **Zhuolong Yang:** Visualization, Data curation. **Youfeng Gao:** Resources, Data curation. **Xuejiao Qu:** Validation. **Haibo Liu:** Investigation. **Yongkang Yin:** Data curation. **Chengshan Wang:** Supervision. **Xiaoqiao Wan:** Resources. **Shumin Chen:** Resources.

## Declaration of competing interest

The authors declare that they have no known competing financial interests or personal relationships that could have appeared to influence the work reported in this paper.

## Data availability

Data will be made available on request.

## Acknowledgments

The authors appreciate support from the International Continental Scientific Drilling Program. This work was supported by the National Natural Science Foundation of China (NSFC No. 41790453, 41472304, 42102129, 42102135 and 41972313), Natural Science Foundation of Jilin Province (20170101001JC), the National Key Research & Development Program of China (2019YFC0605402), and China Geological Survey (DD20189702). We are appreciative for the thorough and valuable comments of Associate Editor Dr. Alexander L Peace, reviewer Dr Ahmed Abdelmaksoud, Dr Mohamed Arab and another two anonymous reviewers, which greatly improved and sharpened logic for our manuscript.

## References

Corti, G., 2009. Continental rift evolution: from rift initiation to incipient break-up in the Main Ethiopian Rift, East Africa. Earth Sci. Rev. 96 (2009), 1–53. https://doi.org/10.1016/j.earscirev.2009.06.005.

Daqing oil and gas region compilation committee, 2023. Petroleum Geology of China, second ed. Petroleum industry press, Beijing.

Davis, G.A., Darby, B.J., Zheng, Y.D., Spell, T.L., 2002. Geometric and temporal evolution of an extensional detachment fault, Hohhot metamorphic core complex, Inner Mongolia, China. Geology (Boulder). 30, 1003–1006. https://doi.org/10.1130/0091-7613(2002)030<1003:GATEOA>2.0.CO;2.

Davis, G.A., Lister, G.S., 1988. Detachment Faulting in Continental Extension; Perspectives from the Southwestern U.S. Cordillera, vol. 218. Special papers (Geological Society of America), pp. 133–159. https://doi.org/10.1130/SPE218-p133.

Feng, Z.Q., Graham, S.A., 2023. From foredeep to orogenic wedge-top: the Cretaceous Songliao retroforeland basin, China. Geosci. Front. 14, 101527 https://doi.org/10.1016/j.gsf.2022.101527.

Franke, D., 2013. Rifting, lithosphere breakup and volcanism: comparison of magma-poor and volcanic rifted margins. Mar. Petrol. Geol. 43, 63–87. https://doi.org/10.1016/j.marpetgeo.2012.11.003.

Fu, W., Hou, H.S., Gao, R., Liu, C., Yang, J., Guo, R., 2019. Fine structure of the lithosphere beneath the Well SK-2 and its adjacent; Revealed by deep seismic reflection profile. Chinese J. Geophys 62, 1349–1361. https://doi.org/10.6038/cg2019M0370 in Chinese.

Fu, Y., Cheng, R.H., Gao, Y.F., Zhou, Y., Xu, Z.J., 2022. Pyroclastic deposition in the cretaceous Shahezi formation (well SK-2) Songliao Basin, China: implications for tectonics and volcanism. Geol. J. 57, 2346–2364. https://doi.org/10.1002/gj.4414.

Gernigon, L., Franke, D., Geoffroy, L., Schiffer, C., Foulger, G.R., Stoker, M., 2020. Crustal fragmentation, magmatism, and the diachronous opening of the Norwegian-Greenland Sea. Earth Sci. Rev. 206, 102839 https://doi.org/10.1016/j.earscirev.2019.04.011.

Gresseth, J.L.S., Osmundsen, P.T., Peron-Pinvidic, G., 2023. 3D evolution of detachment fault systems in necking domains: insights from the Klakk fault complex and the frøya high, mid-Norwegian rifted margin. Tectonics 42, e2022TC007600. https://doi.org/10.1029/2022TC007600.

Li, Z.Q., Chen, J.L., Zou, H., Wang, C.S., Meng, Q.A., Liu, H.L., Wang, S.Z., 2021. Mesozoic-cenozoic tectonic evolution and dynamics of the Songliao Basin, NE Asia: implications for the closure of the Paleo-Asian Ocean and mongol-okhotsk Ocean and subduction of the Paleo-Pacific Ocean. Earth Sci. Rev. 218, 103471 https://doi.org/10.1016/j.earscirev.2020.103471.

Liu, H.B., Wang, P.J., Gao, Y.F., Hou, H.S., Yin, Y.K., Li, H.H., 2021. New data from ICDP borehole SK2 and its constraint on the beginning of the lower cretaceous Shahezi formation in the Songliao Basin, NE China. Sci. Bull. 66, 411–413. https://doi.org/10.1016/j.scib.2020.12.002.

Liu, Y.J., Li, W.M., Feng, Z.Q., Wen, Q.B., 2017. Neubauer F, liang CY, A review of the paleozoic tectonics in the eastern part of central asian orogenic belt. Gondwana Res. 43, 123–148. https://doi.org/10.1016/j.gr.2016.03.013.

Ma, Q., Zhong, Y.T., Yin, Q.Z., Huyskens, M.H., Ma, L., Xia, X.P., Meng, Q.R., Zhou, Z.H., Xu, Y.G., 2024. High-resolution chronostratigraphy of late Mesozoic sequences in northern North China: implications for the linkages among intracontinental orogeny, volcanism, Jehol Biota, and Pacific plate subduction. Geology 52, 45–50. https://doi.org/10.1130/G51535.1.

Ren, J.S., Niu, B.G., Wang, J., Jin, X.C., Xie, L.Z., 2013. International Geological Map of Asia, 1:5000000, Institute of Geology, Chinese Academy of Geological Sciences. Geol. Publ., House, Beijing.

Ritts, B.D., Berry, A.K., Johnson, C.L., Darby, B.J., Davis, G.A., 2010. Early Cretaceous supradetachment basins in the Hohhot metamorphic core complex, Inner Mongolia, China. Basin Res. 22, 45–60. https://doi.org/10.1111/j.1365-2117.2009.00433.x.

Schlumberger, 2018. PetrelTM 2018. https://www.slb.com/products-and-services/delivering-digital-at-scale/software/petrel-subsurface-software/petrel.

Vibe, Y., Bunge, H.P., Clark, S.R., 2018. Anomalous subsidence history of theWest Siberian Basin as an indicator for episodes of mantle induced dynamic topography. Gondwana Res. 53, 99–109. https://doi.org/10.1016/j.gr.2017.03.011.

Wan, X.Q., Zhao, J., Scott, R.W., Wang, P.J., Feng, Z.H., Huang, Y.D., 2013. Late cretaceous stratigraphy, Songliao Basin, NE China: SK1 cores. Palaeogeogr. Palaeoclimatol. Palaeoecol. 385, 31–43. https://doi.org/10.1016/j.palaeo.2012.10.024.

Wang, B., Sun, D.S., Chen, Q.C., Lin, W.R., Li, A.W., Cao, H., 2020. Stress-state differences between sedimentary cover and basement of the Songliao Basin, NE China: in-situ stress measurements at 6–7 km depth of an ICDP Scientific Drilling borehole (SK-II). Tectonophysics 777, 228337. https://doi.org/10.1016/j.tecto.2020.228337.

Wang, C.S., Gao, Y., Ibarra, D.E., Wu, H.C., Wang, P.J., 2021. An unbroken record of climate during the age of dinosaurs. Eos 102. https://doi.org/10.1029/2021EO158455.

Wang, C.S., Gao, Y., Wang, P.J., Wu, H.C., Lv, Q.T., Zhu, Y.Y., Wan, X.Q., Zou, C.C., Huang, Y.J., Gao, Y.F., Xi, D.P., Wang, W.S., He, H.Y., Feng, Z.H., Yang, G., Deng, C. L., Zhang, L.M., Wang, T.T., Hu, B., Cui, L.W., Peng, C., Yu, E.X., Huang, H., Yang, L., Wu, Z.X., 2024. International continental scientific drilling project of the Songliao Basin: terrestrial geological records of the cretaceous dinosaur age. Earth Sci. Front. https://doi.org/10.13745/j.esf.sf.2024.1.4-en.

Wang, P.J., Chen, S.M., 2015. Cretaceous volcanic reservoirs and their exploration in the Songliao Basin, northeast China. AAPG (Am. Assoc. Pet. Geol.) Bull. 99, 499–523. https://doi.org/10.1306/09041413095.

Wang, P.J., Mattern, F., Didenko, N.A., Zhu, D.F., Singer, B., Sun, X.M., 2016. Tectonics and cycle system of the Cretaceous Songliao Basin: an inverted active continental margin basin. Earth Sci. Rev. 159, 82–102. https://doi.org/10.1016/j.earscirev.2016.05.004.

Wang, T.T., Wang, C.S., Ramezani, J., Wan, X.Q., Yu, Z.Q., Gao, Y.F., He, H.Y., Wu, H.C., 2022. High-precision geochronology of the early cretaceous Yingcheng formation and its stratigraphic implications for Songliao Basin, China. Geosci. Front. 13, 101386 https://doi.org/10.1016/j.gsf.2022.101386.

Xie, X.N., Muller, R.D., Li, S.T., Gong, Z.S., Steinberger, B., 2006. Origin of anomalous subsidence along the Northern South China Sea margin and its relationship to dynamic topography. Mar. Petrol. Geol. 23, 745–765. https://doi.org/10.1016/j.marpetgeo.2006.03.004.

Yang, Y.T., Guo, Z.X., Song, C.C., Li, X.B., He, S., 2015. A short-lived but significant Mongol-Okhotsk collisional orogeny in latest Jurassic-earliest Cretaceous. Gondwana Res. 28, 1096–1116. https://doi.org/10.1016/j.gr.2014.09.010.

Yin, Y.K., Gao, Y.F., Wang, P.J., Qu, X.J., Liu, H.B., 2019. Discovery of triassic volcanic-sedimentary strata in the basement of Songliao Basin. Sci. Bull. 64, 644–646. https://doi.org/10.1016/j.scib.2019.03.020.

Yu, T.J., Wang, P.J., Zhang, Y., Gao, Y.F., Chen, C.Y., 2022. Discovery of the late jurassic-early cretaceous lamprophyres in western Songliao Basin of Northeast China and their constraint on regional lithospheric evolution. Front Earthsc-switz 10, 849665. https://doi.org/10.3389/feart.2022.849665.

Yu, Z.Q., He, H.Y., Deng, C.L., Lu, K., Shen, Z.S., Li, Q.L., 2020. New SIMS U-Pb geochronology for the Shahezi formation from CCSD-SK-IIe borehole in the Songliao Basin, NE China. Sci. Bull. 65, 1049–1051. https://doi.org/10.1016/j.scib.2020.03.039.

Yu, Z.Y., Zhang, P.Z., Min, W., Wei, Q.H., Zhao, B., 2018. Cenozoic pulsed compression of Da'an-Dedu Fault Zone in Songliao Basin (NE China) and its implications for earthquake potential: evidence from seismic data. Tectonophysics 722, 383–399. https://doi.org/10.1016/j.tecto.2017.11.013.